Synaptic plasticity during cortical Up-Down state oscillatory activity

Julian Bartram

Corpus Christi College
University of Oxford

A thesis submitted for the degree of
Doctor of Philosophy

Michaelmas 2015

Synaptic plasticity during cortical Up-Down state oscillatory activity

Julian Bartram

Corpus Christi College
University of Oxford

A thesis submitted for the degree of
Doctor of Philosophy

Michaelmas 2015

Abstract

The functions of sleep are diverse and still poorly understood, but a strong effect on cognition is evident. An impressive number of studies suggest that particularly deep sleep, with characteristic cortical slow-wave activity, mediates some important beneficial effects on learning and memory, such as memory consolidation and integration. In the light of this, it is surprising how little we know about the specific rules of synaptic plasticity associated with characteristic activity patterns of different sleep stages.

Therefore, using whole-cell recordings from single or synaptically coupled principal cells and two-photon Ca^{2+} imaging of dendritic spines, I explored how the ongoing network state might promote activity-dependent synaptic plasticity in an *in vitro* model of the medial entorhinal cortex. This experimental setup allowed precise control over Up-Down state oscillations (cellular membrane potential fluctuations associated with slow-wave activity) – a methodological advantage that is difficult to achieve *in vivo*.

I found that evoking subthreshold synaptic inputs during the Up state phase of cortical slow-wave activity induced N-methyl-D-aspartate receptor-dependent synaptic weakening. In fact, the spontaneous, intrinsically generated recurrent network activity that underlies cortical Up states was able to depress the very inputs that help maintain it. These findings are in agreement with the synaptic homeostasis hypothesis of sleep, a proposal for which descriptions of clear molecular and cellular mechanisms have been missing. Next, I investigated spike-timing dependent plasticity during Up state periods. I found that input-correlated postsynaptic spiking can prevent synaptic weakening. This suggests that while subthreshold synaptic inputs become continuously weaker during slow-wave activity, correlated inputs become relatively more dominant – a process that could be related to memory consolidation. Finally, I investigated Ca^{2+} signalling in dendritic spines during Up-Down state oscillations using a novel multi-photon microscope based on the remote-focusing technology. These experiments identified a biochemical signature that could drive the observed plasticity rules.

Acknowledgements

I would like to thank Prof. Edward Mann, a brilliant scientist, who was not only a fantastic supervisor, but also managed to put up with my time management.

I also have to thank the entire Groove Unit for countless discussions and inspirations. It would have been half the fun without you.

Phoebe, you kept me sane during the final weeks. BFK.

I specifically have to acknowledge some members of the Mann group. Martin Kahn assisted with some of the electrophysiological recordings in chapter 3 and provided numerous helpful discussions. The imaging experiments involving the remote-focusing system were conducted within a collaboration between the Mann group, Department of Physiology, Anatomy and Genetics and Prof. Tony Wilson's group, Department of Engineering Science (University of Oxford). Dr. Simon Tuohy is an excellent engineer and scientist, who kept the prototype of the remote-focusing system running. Many of the imaging experiments were conducted in collaboration with Simon.

List of abbreviations

AD Alzheimer's Disease
AMPAR α-amino-3-hydroxy-5-methyl-4-isoxazolepropionic acid receptor
CV coefficient of variation
EC entorhinal cortex
EPSP excitatory postsynaptic potential
GABA gamma-aminobutyric acid
GSK3β glycogen synthase kinase 3 β
LEC lateral entorhinal cortex
LFS low-frequency stimulation
LFP local field potential
LTD long-term depression
LTP long-term potentiation
MEC medial entorhinal cortex
mEPSC miniature excitatory postsynaptic current
NMDAR N-methyl-D-aspartate receptors
NREM non-rapid eye movement (sleep)
PMT photomultiplier tube
REM rapid eye movement (sleep)
RF remote-focusing
SHG second-harmonic generation
SHY synaptic homeostasis hypothesis
STDP spike-timing dependent plasticity
SWA slow-wave activity
SWR sharp-wave ripples
SWS slow-wave sleep
TPEF two-photon excitation fluorescence
VSD voltage-sensitive dyes

List of figures

Contents

1 Introduction

A clear understanding of the functions of sleep remains elusive. Sleep is a behavioural state or process that is evidently needed for normal cognitive performance and health. We are, however, only beginning to isolate the cellular and circuit mechanisms that mediate its beneficial effects. Mounting evidence suggests that sleep is important for the consolidation of memories at the synaptic and systems level (Diekelmann and Born 2010) and the homeostatic renormalisation of synaptic weight (Tononi and Cirelli 2014) – processes that are not necessarily mutually exclusive. To fully understand these phenomena we need to elaborate the rules and mechanisms of synaptic plasticity during the characteristic patterns of brain activity of sleep. The defining cortical activity of *deep sleep* is slow membrane potential oscillations (Steriade, Nunez, and Amzica 1993; Steriade, Timofeev, and Grenier 2001), or *slow waves*, that can travel in synchrony across the cortical mantel (Amzica and Steriade 1995; Sanchez-Vives and McCormick 2000; Massimini et al. 2004). Such slow-wave sleep, which displays rebound following sleep deprivation, might play a critical role in synaptic plasticity and homeostasis (Tononi and Cirelli 2014). Moreover, the consolidation of hippocampus-dependent declarative memories is favoured by early sleep with

heightened slow-wave activity (SWA) (Plihal and Born 1997; Plihal and Born 1999), and can be boosted by inducing slow wave oscillations via transcranial electrical field stimulation (Marshall et al. 2006). SWA is a manifestation of the synchronous fluctuation of the membrane potential of cortical neurons between depolarised *Up states* and hyperpolarised *Down states* (Steriade, Nunez, and Amzica 1993). Up state periods are associated with recurrent network activity during which neurons receive balanced increases in excitatory and inhibitory inputs and often display spiking activity, while Down state periods are mostly quiescent (Sanchez-Vives and McCormick 2000; Shu et al. 2006; Chen et al. 2013). Although activity-dependent synaptic potentiation and depression have been observed during Up-Down state fluctuations (Crochet et al. 2006), their mechanisms and interactions with the ongoing slow-wave phase (Up state vs. Down state) are mostly unknown. It is furthermore still a matter of debate whether these processes might favour global net changes in synaptic weight in one direction or another.

In the next sections of this introductory chapter I will provide a more extended review of the previous body of research that inspired this thesis.

1.1 A role for sleep in learning and memory

An impressive wealth of research suggests that sleep has a variety of beneficial effects on memories acquired during previous waking periods (see

Diekelmann and Born 2010; Rasch and Born 2013). This includes, as already mentioned, prominent improvements in retaining declarative memory, but also extends to the consolidation of emotional and procedural memory (Wagner, Gais, and Born 2001; Stickgold, James, and Hobson 2000; Fischer et al. 2002; Walker et al. 2002). While such a strengthening of initially labile memory is certainly an important feature of sleep, the representation of declarative memories can also undergo a qualitative change during their integration into networks that store already existing memories (Ellenbogen et al. 2007; Lewis and Durrant 2011; Stickgold and Walker 2013). This observation has fueled the discussion on what the underlying mechanisms are that mediate sleep's effects on memory, for which there are two popular (not mutually exclusive) hypotheses: The active systems consolidation hypothesis and the synaptic homeostasis hypothesis.

Active systems consolidation is a conceptually more abstract idea and is based on the two-stage model of memory consolidation, in which new memories are initially and temporarily stored in the hippocampus before they are over time transferred to the cerebral cortex for long-term memory storage (Buzsáki 1989; McClelland, McNaughton, and O'Reilly 1995). Moreover, this transfer is supposedly achieved via the coordinated replay of spike sequences related to memory traces between hippocampal formation and neocortex and, importantly, the resulting consolidation and integration of the memory involves

synaptic potentiation (Born, Rasch, and Gais 2006; Rasch and Born 2013). This model is supported by a functional coupling of the three cardinal oscillations of NREM sleep: slow (0.5 – 2 Hz) cortical Up-Down state oscillations, introduced above, thalamo-cortical sleep spindles [7-14 Hz LFP oscillations preferentially occurring during early SWS (Battaglia et al. 2011)] and hippocampal sharp wave-ripple complexes [aperiodic synchronised network bursts that are accompanied by 150-250 Hz oscillations of the LFP in hippocampal subfield CA1, one of the output structures of the hippocampal formation that projects directly to entorhinal cortex (Buzsáki et al. 1992; Sirota et al. 2003)]. Studies in rodents and humans have consistently found that these oscillations tend to show hierarchical nesting, where spindle activity preferentially occurs during Up state periods and ripples tend to nest in spindle troughs (Siapas and Wilson 1998; Sirota et al. 2003; Staresina et al. 2015). Finally, sharp-wave ripples have been associated with the replay of spike sequences (Wilson and McNaughton 1994; Kudrimoti, Barnes, and McNaughton 1999), providing the last piece of a potential memory transfer model: Here, Up states coordinate a fined-tuned dialog between hippocampus and neocortex resulting in the replay of memory traces during excitatory phases of sleep spindles, which ultimately facilitates synaptic plasticity processes in neocortex, leading to memory consolidation and integration (Diekelmann and Born 2010). However, clear evidence that this orchestrated

replay results in synaptic potentiation in cortex is still lacking. Furthermore, replay could be instead associated with general principles of the circuit architecture and not be related to memory consolidation at all (Buhry, Azizi, and Cheng 2011), and the hippocampus could function as an index for neocortical memories, rather than a temporary storage place, thus not requiring memory transfer.

Another popular hypothesis that seeks to explain the memory function of sleep is the synaptic homeostasis hypothesis, or SHY, mostly developed in the Tononi laboratory (Tononi and Cirelli 2003; Tononi and Cirelli 2006). SHY is more concerned with low-level descriptions of synaptic plasticity, but the proponents have adapted the original proposal to account for the consolidation and integration of memory as well. The core proposal of SHY is that the fundamental function of sleep is the global depression of the net synaptic weight, which is necessary due to the net build-up of synaptic weight during previous waking periods, and thus serves to maintain network synaptic homeostasis. While originally a proportional downscaling of synapses until synapse elimination was suggested, more recent models have included 'down-selection' rules based on activity-dependent plasticity (Tononi and Cirelli 2014). Such a non-uniform depression is essential to account for the integration of memories, since SHY proposes that synaptic potentiation is rare during sleep, and that the neuromodulatory milieu and gene expression levels

are rather geared to facilitate synaptic depression. A vast number of molecular and structural findings in different species are consistent with the key proposal of SHY. The most convincing studies include the observation that changes of the early slope of cortical evoked responses and the amplitude of mEPSCs, both measures of synaptic strength, increase during wakefulness and decrease during sleep (Vyazovskiy et al. 2008; Liu et al. 2010). Similarly, molecular markers of synaptic potentiation (e.g. AMPAR subunit composition and phosphorylation states of AMPARs, CamKII and GSK3β) are up-regulated after wakefulness compared to the end of sleeping periods (Vyazovskiy et al. 2008), while the reverse was found for a marker of synaptic depression (AMPAR dephosphorylation at Ser845) (Hinard et al. 2012). Structural two-photon imaging studies in early adolescent mice showed that net elimination of dendritic spines and filopodia prevailed during sleep (Maret et al. 2011; Yang and Gan 2012). This net elimination of protrusions was not seen in adult mice, although this does not preclude synaptic homeostasis via changes in synaptic strength at older ages (Maret et al. 2011).

However, the evidence in support of SHY is not equivocal, and the hypothesis remains controversial (Frank 2013). While the hypothesis is relatively vague, and can be refined to interpret the evidence from diverse studies (Tononi and Cirelli 2014), it does have fundamental problems in

accounting for experiments suggesting increases in synaptic weights following sleep. For example, it was recently found that sleep after a task involving motor skill learning can promote the growth of new spines in motor cortex, which are subsequently protected from elimination (Yang et al. 2014). Moreover, *Yang et al.* provide some evidence that this may depend on neuronal replay during NREM sleep. In the end it is conceivable that some aspects from both the active system consolidation and synaptic homeostasis hypothesis are implemented in order to mediate – likely in conjunction with other undiscovered mechanisms – sleep's beneficial effects on memory.

The importance of deep NREM sleep for active systems consolidation has already been highlighted above. Furthermore, slow-wave activity, a reliable indicator of sleep need, has also been implicated in directly mediating synaptic homeostasis (Tononi and Cirelli 2014): Accordingly, SWA is high at the beginning of sleep, potentially reflecting strong synaptic potentiation after learning, and decreases during sleep at least partially due to global synaptic depression. This is further supported by particularly strong local increases in SWA in task-relevant cortical regions during sleep following learning (Hanlon et al. 2009). In this thesis I focused on examining synaptic plasticity during cortical SWA, characteristic for deep NREM sleep, because there is sufficient evidence suggesting a critical role in learning and memory as outlined above. Elaborating the function of REM sleep periods on the other hand has proven

to be more difficult and even their necessity has been challenged by the observation that suppression of REM sleep by antidepressants or brain lesion did not result in obvious impairments (Siegel 2001). Whether a role of REM sleep is, for example, the 'selection' of networks to evaluate the 'recovery' (including synaptic homeostasis) during previous NREM sleep (Vyazovskiy and Delogu 2014) or, perhaps, the potentiation of synapses that were 'tagged' as a result of memory replay (Rasch and Born 2013) remains to be seen.

Taken together, a role for NREM sleep in learning and memory is compelling. However, what underlying forms of synaptic plasticity might be promoted is less clear. After a brief introduction to the main cell type examined in this project in the next section, mechanisms of synaptic plasticity during SWA will be critically discussed in the context of the above proposals for the memory function of sleep.

1.2 MEC layer III principal cells: role in the EC-hippocampal circuitry and importance for sleep-dependent neocortical-hippocampal interaction

In this study, I investigated synaptic plasticity at synapses onto spiny principal cells in layer III of the mouse medial entorhinal cortex. While the goal was to identify mechanisms that may extend to different cortical layers and areas, this cell type and region was not randomly chosen, but it was influenced by

evidence that indicate a particularly important role of MEC layer III principal cells in mediating the neocortical-hippocampal dialog. MEC layer III principal cells receive strong cortical afference and provide main projections to hippocampal area CA1 (Canto, Wouterlood, and Witter 2008). Astonishingly, in vivo recordings in mice during anaesthesia and SWS showed that MEC layer III cells can skip several neocortical Down states, thus producing long, persistent Up states (Hahn et al. 2012). This suggests that the MEC circuitry can temporarily decouple from neocortex and act as an independent pattern generator during SWS. Interestingly, *Hahn et al.* continued to show that it is this persistent activity that drives CA1 neurons explaining the apparent desynchronisation of hippocampal and neocortical activity during SWS. These findings are complemented by the identification of superficially projecting layer V principal cells in entorhinal cortex (van Haeften et al. 2003; Canto, Wouterlood, and Witter 2008). MEC layer V principal cells preferentially receive output from the hippocampus and direct projections from layer V to layer III would close a loop within the EC-hippocampal circuitry that could allow a dialog between EC and hippocampus during persistent Up states that is temporarily decoupled from neocortex. Such a dialog could be important for the initialisation of spike replay. Sharp-wave ripples are generated intrinsically in CA3, propagate to CA1, and finally result in synchronised activity in deep layers of EC (Chrobak and Buzsáki 1996). Thus, over several neocortical

slow-wave cycles, ripple-associated replay could be coordinated or information pre-processed within the EC-hippocampal system before communication with neocortex. Furthermore, MEC layer III principal cells could provide a distinct stream of information to hippocampus. This was influenced by the idea that MEC and lateral entorhinal cortex (LEC) – both providing CA1 input – could represent spatial and nonspatial information, respectively, and the observations that LEC cells do not exhibit persistent Up states (Hahn et al. 2012). Therefore, depending on whether MEC layer III principal cells enter a persistent Up state or not, CA1 would have distinct streams of information available (Dupret and Csicsvari 2012).

These findings demonstrate that MEC layer III principal cells occupy a critical role within the EC-hippocampal system and are likely to have an important function within the circuitry that mediates aspects of learning and memory.

1.3 Synaptic plasticity during cortical slow-wave activity – a brief review

Slow oscillations can have profound effects on transforming the neuronal output including short- and long-term synaptic plasticity as well as changes in intrinsic excitability (Steriade and Timofeev 2003; Timofeev 2011). In this

section, I will discuss activity-dependent forms of synaptic plasticity during SWA that might contribute to mediating the beneficial effect of sleep on learning and memory. The hallmarks of cortical Up states – increased synaptic activity, membrane potential depolarisation and action potential firing – could indeed promote numerous types of changes in synaptic weight: For example, Hebbian plasticity, which involves coordinated pre- and postsynaptic activity (Hebb 1949). In fact, shortly after the first discovery of a long-lasting strengthening of synapses termed long-term potentiation or LTP (Bliss and Lømo 1973; Bliss and Gardner-Medwin 1973), depolarisation of the postsynaptic cell was quickly identified to be critical for the induction of plasticity (Kelso, Ganong, and Brown 1986; Sastry, Goh, and Auyeung 1986; Gustafsson et al. 1987). Moreover, a role of the precise timing of presynaptic and postsynaptic spikes in determining the sign of plasticity was established (Markram et al. 1997; Bi and Poo 1998; Zhang et al. 1998). More recently, a unified model was developed that has the relationship of presynaptic spike timing and postsynaptic voltage at its core and can account for many experimentally observed changes of synaptic strength (Clopath and Gerstner 2010). The originally discovered form of LTD, however, did not agree with Hebb's postulate and instead was a type of ('anti-Hebbian') heterosynaptic plasticity that was induced at inactive synapses by the activity of neighbouring inputs (Lynch, Dunwiddie, and Gribkoff 1977; Levy and Steward 1979). Soon

after these discoveries homosynaptic LTD induced by low-frequency stimulation of afferent fibres was found (Barrionuevo, Schottler, and Lynch 1980), and in the following years studies revealed LTD in many regions and cell types of the central nervous system with diverse induction and expression mechanisms (Massey and Bashir 2007). Taken together, changes in synaptic strength during cortical SWA could potentially be mediated by an impressive variety of plasticity forms.

Given the plethora of different rules for synaptic plasticity that could be engaged during Up/Down states, resolving the functions of SWA activity in synaptic plasticity will require 'real-time' intracellular recordings. Unfortunately, very little data exists, and the few available studies have painted an unclear picture. During SWA in cat cortex in vivo and in vitro, electrical stimulation of local and projecting pathways at frequencies similar to endogenous sleep oscillations (including spindle-like activity) resulted during some experiments in synaptic potentiation and others in synaptic depression (Cissé et al. 2004; Crochet et al. 2006). Examining the influence of the degree of SWA on the direction of plasticity, it was concluded that high levels of SWA promote synaptic potentiation (Crochet et al. 2006). However, the fact that it was not further analysed whether the network was in an Up state during plasticity induction, or if afferent stimulation was in any way correlated with postsynaptic spiking, makes the interpretation of these results difficult: as

discussed above, postsynaptic depolarisation or correlated input-spike pairings can have profound effects on the induction of synaptic plasticity. Indeed, the only study I am aware of in which synaptic strength and Up/Down states were carefully monitored and controlled revealed that single spikes positively correlated with synaptic activity during Up state periods can lead to a relative synaptic potentiation to input-spike pairings applied during Down state periods (Kruskal, Li, and MacLean 2013).

The weak direct evidence that does exist points to a role of SWA in synaptic potentiation, or at least confirms that synaptic potentiation can occur. A cellular learning rule that would preferentially drive synaptic depression during Up/Down states can only be inferred from indirect evidence and modelling data. Here, I highlight five potential mechanisms that could mediate a sleep-dependent reduction in synaptic strength:

(i) SWR-dependent depression

In vitro studies suggest that a subpopulation of principal cells could undergo synaptic downscaling by the trigger of ectopic action potentials during, surprisingly, sharp-wave ripple activity (Papatheodoropoulos 2008; Bukalo et al. 2013). However, these findings could depend on artificial recording conditions and would be restricted to CA1.

(ii) Input-correlated or repetitive bursting

In somatosensory cortex of rodents at synapses on layer V principal cells, a long-term depression and AMPA receptor removal by input-correlated postsynaptic bursting or repetitive bursting has been identified and proposed to underlie synaptic homeostasis during SWA that exhibits a high frequency of Up state-associated bursting (Birtoli and Ulrich 2004; Czarnecki, Birtoli, and Ulrich 2007; Lanté et al. 2011). These findings are confronted with numerous classic descriptions of burst-LTP rather than LTD for positive pairings (see above) and, moreover, both mechanisms are naturally limited to principal cells that show frequent bursting activity. It is therefore questionable how ubiquitous such a homeostatic depression mechanisms could be. Finally, the effect of pairing a burst-LTP protocol with an Up state period has to my knowledge not been studied to date.

(iii) Reversal of STDP rules

Yet another plasticity rule based on spike-timing dependent plasticity (STDP) that has been successfully implemented in a neural network model to achieve a global trend towards synaptic depression assumes a change of STDP polarity induced by a neuromodulatory milieu typical for NREM sleep (Olcese, Esser, and Tononi 2010). Although the authors discuss some support by experimental findings, a global reversal of the STDP sign appears to be an optimistic assumption and has, at least in one case, not been experimentally observed (Kruskal, Li, and MacLean 2013).

(iv) Asymmetric STDP

A more fundamental – yet speculative – depression mechanism to achieve synaptic homeostasis that could influence the majority of synapses that contribute to Up state periods might simply rely on asymmetric windows for spike-timing based LTD (t-LTD) and LTP. Windows of input-spike delays can be wider for LTD compared to LTP induction, and as a consequence it was found that repeated activation of a synapse paired with a postsynaptic spike at random delays results in a gradual synaptic depression of the activated input (Feldman 2000). Hence, inputs that contribute to Up states showing spiking activity could be gradually depressed in the course of SWS. This process could even be supported by inhibitory conductances that help balancing Up states. Using two-colour uncaging of glutamate and GABA it was recently found that by controlling Ca^{2+} signalling localised GABAergic inhibition could strongly promote spine shrinkage induced by a t-LTD protocol (Hayama et al. 2013). This reduction in spine size, potentially a structural correlate of LTD, even spread to neighbouring spines. Dendritic inhibitory cells, such as somatostatin-expressing interneurons, show spiking activity during Up states in entorhinal cortex and other areas and, interestingly, pyramidal cells show a dominant peak of inhibitory conductances in the early Up state phase (Neske, Patrick, and Connors 2015). Whether such mechanisms based on wide windows for spike-timing dependent LTD are in

place remains to be shown. Depending on the brain region and cell type, however, some cells do not exhibit any Up state-associated spiking activity and could therefore not exploit STDP for synaptic homeostasis.

(v) Subthreshold pairings

Mechanisms of synaptic depression that are independent of postsynaptic spiking are conceivable too: For example, LTD was induced at neocortical layer V - layer V connections of principal cells by pairing presynaptic activity with postsynaptic subthreshold depolarisation (Sjöström, Turrigiano, and Nelson 2004). For plasticity induction, the postsynaptic cell was depolarised by brief current injection to approximately 15 mV above resting membrane potential – a voltage step that is intriguingly similar to Up state periods.

In this section, I tried to highlight the limited information we currently have about the rules and mechanisms of synaptic plasticity that could operate during SWS. Single-spike and burst-STDP might occur, but how these processes are influenced by Up state periods is less clear. Mechanisms of synaptic plasticity that have been proposed to mediate synaptic homeostasis were discussed and their limitations highlighted. Finally, some speculative suggestions for more wide-ranging mechanisms of synaptic depression that could achieve synaptic homeostasis were introduced.

1.4 Objective of this thesis

In this thesis project, I investigated the rules and mechanisms of synaptic plasticity during cortical Up-Down state oscillations at synapses onto spiny principal cells in layer III of the mouse medial entorhinal cortex. The specific goals were as follows:

1. **Investigate the effect of pairing subthreshold synaptic activity with cortical Up state periods on synaptic strength, and elucidate the underlying mechanistic details.**

2. **Determine the role of postsynaptic spiking in Up state-associated synaptic plasticity.**

3. **Establish remote-focusing (RF) two-photon microscopy for routine imaging of neural activity.**

4. **Use the RF technology to image dendritic Ca^{2+} signals during Up-Down oscillations, and link results to mechanisms of Up state-associated synaptic plasticity.**

2 Materials and methods

2.1 Animals

All procedures were carried out in accordance with the UK Animals (Scientific Procedures) Act of 1986. Only the C57BL/6 inbred mice strain was used and animals were purchased from Harlan Laboratories, UK. All experiments in this thesis are based on acute-slice preparations from juvenile mice/mice in early adolescence (postnatal day P14-P21). Since these animals were in a pre-weaning stage stress was avoided by leaving the pups with their mother until just before decapitation. Mice were scarified at the end of the normal (adult) waking periods early in the morning. While sleep of young animals is typically more fragmented, most pups were also awake and often showed exploratory behaviour before they were separated from their mother. This helped assuring that the network state *in vitro* resembled early sleep phases with heightened slow-wave activity (Nelson et al. 2013; de Vivo et al. 2014). The focus on juvenile/early adolescent mice can be justified by certain characteristics of this developmental stage, namely sleep with high SWA (Nelson et al. 2013) and intensive learning demands. I did examine whether it would also be possible to explore the mechanisms of synaptic plasticity during SWA in slice preparations from adult mice. However, while some of my initial experiments

indicated that SWA can be achieved in adult acute-slice preparations, Up state generation was unreliable and the Up state duration and amplitude were typically smaller compared to *in vivo* characteristics (data not shown). To my knowledge there is no published study investigating SWA in cortical slices from adult mice, suggesting that this is a common methodological limitation across laboratories. In this thesis, I therefore limited my investigations to young animals.

2.2 Horizontal acute-slice preparation from entorhinal cortex

Horizontal brain slices (350 µm) from young/early adolescent C57BL/6 mice were prepared after decapitation under deep isoflurane-induced anaesthesia. Slices were dissected in ice-cold artificial CSF (aCSF) containing (in mM): 126 NaCl, 3.5 KCl, 1.25 NaH_2PO_4, 1 $MgSO_4$, 2 $CaCl_2$, 24 $NaHCO_3$, and 10 glucose, at pH 7.2-7.4 when bubbled with carbogen gas (95 % O_2, 5 % CO_2). After initial recovery (> 1 h) in an interface chamber in room temperature carbogenated aCSF, all experiments were conducted under submerged conditions at approximately 33 °C. Previous work has suggested that aCSF with relatively low Mg^{2+} and Ca^{2+} concentrations (< 2 mM) is critical to achieve a level of network excitability that allows the generation of slow-wave activity

(Sanchez-Vives and McCormick 2000; Cunningham et al. 2006). I found that following these recommendations regarding a low Mg^{2+} concentration, but keeping the Ca^{2+} concentration at a more typical value, as listed above, virtually abolished spontaneous Up states, but still allowed the electrical induction of a single Up state (see main text). Given the requirements for exquisite control of both Up and Down states during the experiments, I proceeded with this aCSF composition throughout.

2.3 Electrophysiology

2.3.1 Whole-cell patch-clamp recordings

Whole-cell patch-clamp recordings were obtained with standard borosilicate glass micropipettes (6-8 MΩ) containing (in mM): 110 potassium-gluconate, 40 HEPES, 2 ATP-Mg, 0.3 GTP, 4 NaCl (pH 7.2; 270–290 mOsmol l^{-1}). Biocytin (Sigma-Aldrich) was added at 4 mg ml^{-1}. Current-clamp recordings were carried out using an Axon Multiclamp 700B amplifier (Molecular Devices) and ITC-18 A/D board (Instrutech) (all experiments that did not involve two-photon microscopy) or an Axon Multiclamp 700A together with an Axon Digidata 1440A digitizer (for electrophysiology experiments in conjunction with two-photon microscopy). I implemented data acquisition and stimulation protocols using IgorPro's (WaveMetrics) proprietary programming language or

the software package Axon pClamp, respectively. The signal was low-pass filtered at 2 kHz and acquired at 10 kHz. The input resistance (R_i) was determined by a hyperpolarising 20 pA step for 300 ms in each sweep: an exponential curve was fitted to the initial voltage response and with the horizontal asymptote as the maximal response R_i was simply calculated with Ohm's law. Experiments were excluded if the input resistance changed by more than 30 % or the membrane potential (V_m) drifted by more than 10 mV compared to baseline.

2.3.2 Paired-recordings from synaptically coupled principal cells

For paired recordings from synaptically coupled cells, both patch electrodes were placed just over the two selected cells first, followed by quick breakthroughs to avoid unnecessary cell dilution. The connection probability of cortical principal cells typically decreases with increasing distance between the cells (e.g. Holmgren et al. 2003; Levy and Reyes 2012). Hence, the distance between the somata of all tested pairs was chosen to be less than approximately 150 µm. I found that two layer III principal cells were connected with a very low probability of 6.5 %. A previous study in entorhinal cortex of the rat (Dhillon and Jones 2000) reports a slightly higher connection probability of 8.4 % of principal cell layer III-III connections and finds a failure rate of synaptic transmission of approximately 30 % (at 0.2 Hz stimulation) as

opposed to the hardly measureable failure rate of the cells investigated here. While several experimental variables could explain these differences, it might indicate a bias towards stronger, potentially polysynaptic connections since I initially assessed connectivity by using an oscilloscope.

2.3.3 Simultaneous whole-cell patch-clamp and local field potential recordings

To ensure that the Up states I observed are not intrinsically generated, but actually network-driven events, I initially performed simultaneous whole-cell and local field potential (LFP) recordings to verify that there is a coincidental increase in activity in both channels. For the LFP recordings we used the second channel of the Multiclamp 700B - ITC-18 A/D setup as described above. The LFP signal was low-pass filtered at 300 Hz. Borosilicate glass micropipettes with a resistance of approximately 2 MΩ were used and the tip was positioned approximately 150-200 µm away from the patched cell and lowered approximately 50 µm deep into the tissue. [That the observed Up states are indeed network-driven was further supported by the observation that in all paired-recording experiments as described above (108 tested pairs of principal cells) Up state initialisation and termination was quasi simultaneous in both cell.]

2.4 Identification of MEC layer III principal cells

Cells were identified based on electrophysiological characteristics and cell morphology. For a morphological characterisation most slices were fixed in 4% paraformaldehyde (PFA) in phosphate buffered saline (PBS) for at least 1 h (up to 24 h), then 3x washed in PBS, followed by labelling of the patched cells with an avidin, Texas Red conjugate (Life Technologies) and visualisation under a fluorescence microscope. In experiments involving two-photon microscopy, the cell morphology was directly determined by imaging the structural dye, Alexa Fluor 594 (Life Technologies), which was included in the patch-pipette. All cells included in this work have morphological and electrophysiological characteristics that agree with previously published studies on MEC layer III principal cells (Gloveli et al. 1997; van der Linden and Lopes da Silva 1998; Canto, Wouterlood, and Witter 2008): Cell somata were closely located to the *lamina dissecans* and had a pyramidal shape with several basal dendrites and a thick apical dendrite extending towards layer I. Dendrites typically displayed spines. The apical dendrite bifurcated at different positions within layer II and often ended in a layer I tuft (see **Appendix** for some representative high-resolution example cells from several different experiments included in this thesis). Neurons displayed regular spiking characteristics during step protocols, but occasionally showed short bursts

during Up state periods consistent with recordings from MEC layer III principal cells from juvenile animals (Sheroziya et al. 2009). All characteristics taken together, cells are of Type 1 or Type 2 according to the classification of MEC layer III cells by (Gloveli et al. 1997).

2.5 Afferent stimulation and Up state induction

Afferent inputs to layer III principal cells were stimulated with a tungsten electrode placed in the upper region of layer V close to the *lamina dissecans* adjacent to the recorded cell (0.1 ms, 50-100 µA). I selected, if possible, for small EPSPs without obvious inhibitory components (during Down state measurements), which were likely evoked by stimulation of extrinsic inputs and critical intrinsic connections, including superficially projecting layer V principal cells and antidromically activated local layer III principal cells (van Haeften et al. 2003; Canto, Wouterlood, and Witter 2008; Gloveli et al. 1997). Local synaptic stimulation during spine Ca^{2+} imaging was achieved with a micropipette filled with aCSF and Alexa 594 (40 µM) for placement under the two-photon microscope. Stimulus artefacts were occasionally trimmed for better visibility of data.

As described previously (Mann, Kohl, and Paulsen 2009), single Up states were evoked with a tungsten electrode placed in MEC layer III (0.1 ms,

50-200 µA pulses) – typically more than 200 µm away from the recorded cell(s). In Up state pairing protocols (*Fig. 1d iii* and *Fig. 8*), Up states were evoked 100 ms before the first afferent stimulus. This was to ensure that the entire stimulus train will fall into the plateau phase of the Up state despite variations in Up state duration. In spine Ca^{2+} imaging experiments (*Fig. 13*), Up states were evoked 400-500 ms before synaptic activation was triggered. Plasticity protocols consisted of a total number of 50 or 100 pairings. The inter-stimulus interval within trains of stimuli was chosen to be 200 ms to minimise the interaction between the postsynaptic responses.

In the presynaptic cell in paired recording experiments (*Fig. 7*) and for input-spike pairings (*Fig. 1d iii*), action potentials were evoked by brief somatic current injection (5 ms and 10 ms duration, respectively; typically < 1 nA). Brief action potential bursts (2-4 action potentials) (*Fig. 6*) were elicited by slightly longer somatic current injection (2 - 22 ms after afferent stimulation; < 1 nA).

2.6 Automatic detection of the Up state duration

In some experiments, the exact duration of Up states needed to be determined. I used an automated detection algorithm implemented in Igor Pro (WaveMetrics) exploiting the increase in membrane potential noise associated

with Up states to define the duration of an Up state in an unambiguous way: Voltage traces were median filtered (50 point window) and the membrane potential noise was calculated as the running SD over a 200 ms window. The Up state start was simply defined as the time of the induction stimulus. The Down state transition was initially detected as a decrease in membrane potential noise below 3 SD above the baseline mean, lasting for a minimum duration of 500 ms. The end of the Up state was then defined as the point at which the membrane noise had decreased to the baseline mean, or, if this fell into a phase of afterhyperpolarisation, as the preceding time point at which the membrane potential reached the value of the pre-Up state membrane potential. The Up state end detected in this way was visually inspected, and manually corrected in a small minority of traces.

2.7 Pharmacology: NMDAR blockade and GSK3β inhibition

In some experiments (*Fig. 8a*), 200 µM of the NMDA receptor antagonist MK-801 (Sigma-Aldrich) was added to the internal solution. Higher concentrations of MK-801 (> 500 µM), which have commonly been used in the literature, caused a reliable, unexplained change in input resistance. However, even at the relatively low concentration used here a statistically significant reduction of

synaptic weakening was observed (*Fig. 8a*). In agreement with previous *in vivo* findings (Chen et al. 2013), Up state induction (> 5 mV amplitude; > 1 s duration at the time of pairing) was still possible in the presence of MK-801.

In another set of experiments (*Fig. 8b*) 10 µM of the GSK3β inhibitor SB415286 (Abcam) was included in the internal solution. A stock solution of 100 mM SB415286 was prepared in DMSO, and aliquots stored at -20 ^{o}C. A fresh aliquot was used for each experiment, and dissolved 10000-fold in internal solution to give a final concentration of DMSO of 0.01 %. The same volume of DMSO dissolved in internal solution was used as the vehicle control. Again, Up state induction was not impaired. It needs to be said that there are two GSK isoforms (GSK3α and GSK3β) expressed in the mammalian brain (Woodgett 1990). SB415286 inhibits both isoforms and also has some minor inhibitory function at other kinases (Bain et al. 2007). Because of the comparably high expression levels of GSK3β in brain tissues (Lau et al. 1999; Yao et al. 2002) this isoform is generally considered to be the critical one in regulating synaptic plasticity (e.g. Peineau et al. 2007; however, see also Shahab et al. 2014). That is why GSK3β is generally referred to as the main target of SB415286 in this thesis, although one needs to keep in mind the possibility that a different kinase could contribute to the processes discussed in this thesis.

2.8 Remote-focusing two-photon microscopy

2.8.1 Technical specifications

We used a custom-built multi-photon microscope based on the remote focusing technology (Botcherby et al. 2012) for all imaging experiments. The laser source used was a pulsed Ti:Sapphire laser (Tsunami, Spectra Physics) with a peak wavelength of 850 nm. The laser power was adjusted to approximately 300 mW (this was measured before the beam entered the scanning system). A 40x water-objective with a numerical aperture (NA) of 0.8 (Olympus) was employed for live-cell two-photon imaging and some initial second-harmonic generation (SHG) imaging experiments, while a 40x/1.15 NA water-objective (Olympus) was used for high-resolution imaging of fixed slices. Some innovative aspects of this novel remote-focusing system are introduced in *chapter 5*.

2.8.2 Single spine activation and Ca^{2+} imaging of basal dendrites

For spine Ca^{2+} imaging experiments, cells were loaded with the calcium indicator Fluo-5F (400 µM) or Oregon Green 488 BAPTA-1 (OGB-1; 200 µM) and Alexa Fluor 594 (40 µM) for at least 30 minutes. Fluo-5F at the stated concentration was chosen so responses would fall into an appropriate indicator range (Yasuda et al. 2004). All experiments were conducted at approximately 33 °C. Line-scans were performed through spine heads and

the adjacent dendritic shafts every 10 - 15 s. Scan rates varied, mostly depending on the length of the scan path, and were in the range of approximately 30-200 Hz, which is appropriate for the slow kinetics of Ca^{2+} signals. The stimulus strength for local synaptic activation was adjusted to keep postsynaptic responses as small as possible. I observed transmission failures, and I never saw Ca^{2+} transients in spines adjacent to the imaged spine, further supporting the notion that only very few and perhaps only a single synapse was activated. Spontaneous Ca^{2+} transients during Up states in the imaged spine were only seen in one recording and were clearly separated from the evoked response. Individual spine Ca^{2+} responses were expressed as the relative change in fluorescence $\Delta F/F$. We typically recorded less than twenty responses in total per spine to avoid any effects of synaptic weakening and phototoxicity. Only successful synaptic transmissions were included in the analysis (peak Ca^{2+} response > 2.5x the standard deviation of the baseline noise). Raw Ca^{2+} transients (n = 2 - 5) from each group (Up state vs Down state) were averaged and the spine head response was then quantified as the mean $\Delta F/F$ of the initial 400 ms period. Example images of line-scans were filtered with a 3x3 Gaussian kernel, and a 10-pass Gaussian filter was applied to example traces of mean Up and Down state responses.

2.8.3 Imaging spontaneous spine Ca^{2+} transients during Up states

Although some spines remained inactive during Up states, which was exploited as described in the previous section to compare Up state vs Down state responses, some spines showed spontaneous Ca^{2+} transients, which was likely due to excitatory synaptic activation driving the Up state. Spine Ca^{2+} imaging was performed as described above using Fluo-5F at the stated concentration. Spines were randomly selected from the midsection of a basal dendrite. A scan path within 3-dimensional space through several spine heads and the adjacent dendritic shaft was typically defined and tested for active spines by triggering 3-4 Up states. Active spines were typically deeper than 50 µm in the tissue, possibly reflecting the higher chance of axons being cut in more superficial areas. Onset latencies of the spine Ca^{2+} transients (time point at which the signal is for the first time greater than four times the standard deviation of the baseline) were determined in relation to the Up state onset. The probability histogram of normalised onset latencies of Ca^{2+} transients was calculated as follows: In two out of the three experiments that were included in the analysis the spine Fluo-5F fluorescence was imaged during the entire Up state and the Ca^{2+} transient onset latencies were normalised to the respective Up state duration. In one experiment Fluo-5F fluorescence was not imaged during the entire Up state (however, at least during 50% of the Up state duration). In this case the onset latencies were

normalised to the maximum imaging duration. Therefore, strictly speaking, the probability histogram of onset latencies should only be used to identify uniform trends of different latency probabilities in course of the Up state duration. Owing to the fast kinetics of Fluo-5F, it was occasionally possible to resolve two or three 'peaks' in a single Ca^{2+} trace, probably corresponding to several individual presynaptic action potentials or bursts. These extra transients were included in the analysis if there was a point in time between the extra peak and the previous transient at which the signal fell below four times the standard deviation of the baseline noise again. This advantage in terms of temporal resolution might be the main reason for the differences in the results compared to the report by (Chen et al. 2013).

2.9 Data analysis and statistics

Change in synaptic strength was quantified as the baseline-normalised mean EPSP slope (single cell recordings) or mean EPSP amplitude (dual cell recordings) of the ten-minute period starting thirteen or twenty-five minutes, respectively, after the first pairing.

The background and pitfalls of a coefficient of variation (CV) analysis are detailed in *chapter 4*.

Data were analysed with Igor Pro (WaveMetrics) and statistics was done with Prism (GraphPad Software). The respective statistical tests applied (paired and unpaired Student's t-Test, as appropriate, and a one-way analysis of variance) are stated for each experiment in the respective results section.

3 Synaptic plasticity during cortical slow-wave activity

3.1 Introduction

In the previous chapter, I highlighted our limited understanding of how ongoing Up/Down states modulate synaptic weights in cortical networks. To my knowledge, this has specifically not been examined in relation to sleep homeostasis in entorhinal cortex – a key interface between hippocampus and neocortex, which is likely to be critical for any transfer and/or consolidation of memories during sleep. Studying such cellular learning rules in slices enables exquisite control over network activity and afferent stimulation, in addition to enabling long-term stable whole-cell recordings of visually-identified neurons and precise pharmacological manipulation.

In this chapter, I first validated the slice model for generating Up/Down states in mouse medial entorhinal cortex that was used throughout this thesis. I then investigated if repeated subthreshold activity during Up state or Down state periods can induce synaptic plasticity. Finally, timing-based single-spike and burst potentiation of synapses during Up state periods were examined.

3.2 Synaptic weakening and maintenance at synapses onto medial entorhinal cortex layer III principal cells

As discussed in the previous section, synaptic plasticity at synapses onto MEC layer III principal cells was studied throughout this thesis. Importantly, from an experimental point of view, weak electrical stimulation in layer III in acute-slice preparations of the entorhinal cortex can induce a single, localised slow-wave cycle (Mann, Kohl, and Paulsen 2009): a synchronous, network Up state followed by return to a Down state. Under our experimental conditions, the frequency of spontaneous Up-Down state transitions was strongly dependent on the extracellular Ca^{2+} concentration, and at 2 mM Ca^{2+} in the extracellular medium spontaneous Up states were mostly absent (0.0046 Hz, n = 5; continuous ten-minute recordings), while electrical Up state induction was still reliable (**Fig. 1a/b**). This allowed precise control over Up state timing and, at the same time, kept potential plasticity processes associated with spontaneous slow waves to a minimum. Evoked Up states typically had amplitudes > 10 mV and persisted often over several seconds consistent with previous *in vitro* and *in vivo* recordings from MEC layer III principal cells (Mann, Kohl, and Paulsen 2009; Cunningham et al. 2006; Hahn et al. 2012). That the observed Up states are in fact a cellular manifestation of a network-driven slow wave was evident by a coinciding increase in the cell membrane

potential, an increase in membrane potential variability, and slow negative deflections in the simultaneously recorded local field potential from layer III (**Fig. 1c**). Afferent inputs to layer III principal cells were stimulated with a tungsten electrode placed in the upper region of layer V adjacent to the recorded cell (**Fig. 1a**; see also **Methods**).

As discussed in chapter 1, postsynaptic depolarisation is crucial for many types of activity-dependent synaptic plasticity. Since SWA is associated with a bistable fluctuation of the membrane potential of neurons, we wondered if a simple pairing of synaptic activity with the relatively depolarised Up state might suffice in inducing plasticity. To investigate this, excitatory postsynaptic potentials (EPSPs) were evoked by afferent stimulation every 15 s during a 'Down state' (at the resting membrane potential of the cell). Following the recording of a stable baseline, different pairing protocols were applied (**Fig. 1d**). First, we tested if repeated activation of a synapse (stimulus trains at 5 Hz) during a Down state has any effect on synaptic strength (**Fig. 1d *i***). A pairing of 50 afferent activations with a Down state changed the EPSP slope only marginally to 102.6 ± 4.1 % (n = 6). However, when afferent stimulation was paired with evoked Up states (**Fig. 1d *ii***), the synaptic strength, as measured by the EPSP slope, was in fact significantly reduced to 65.9 ± 6.9 % of the baseline value ($p < 0.05$ cf Down state pairing; One-way ANOVA followed by a Tukey posthoc test; n = 6, 9). Finally, I addressed the effect of

pairing postsynaptic spikes with synaptic inputs during Up states (**Fig. 1d *iii***). It is unclear to what extent classic spike-timing dependent plasticity (STDP) rules apply during sleep, and even a reversal of the sign of plasticity during SWA has been suggested (Olcese, Esser, and Tononi 2010). In agreement with a recent study in barrel cortex (Kruskal, Li, and MacLean 2013), we found that input-correlated spiking during Up state pairings does not result in a reversal of the plasticity sign (**Fig. 1d *iii***). Instead, synaptic weakening as seen in *Fig. 1d ii* was prevented and, after an initial trend towards potentiation, a final insignificant increase in the EPSP slope to 109.7 ± 3.5 % was observed ($p < 0.05$ cf Up state pairing; n.s. cf Down state pairing; One-way ANOVA followed by a Tukey posthoc test; n = 6, 9). A summary of these results and statistics are shown in (**Fig. 1e**).

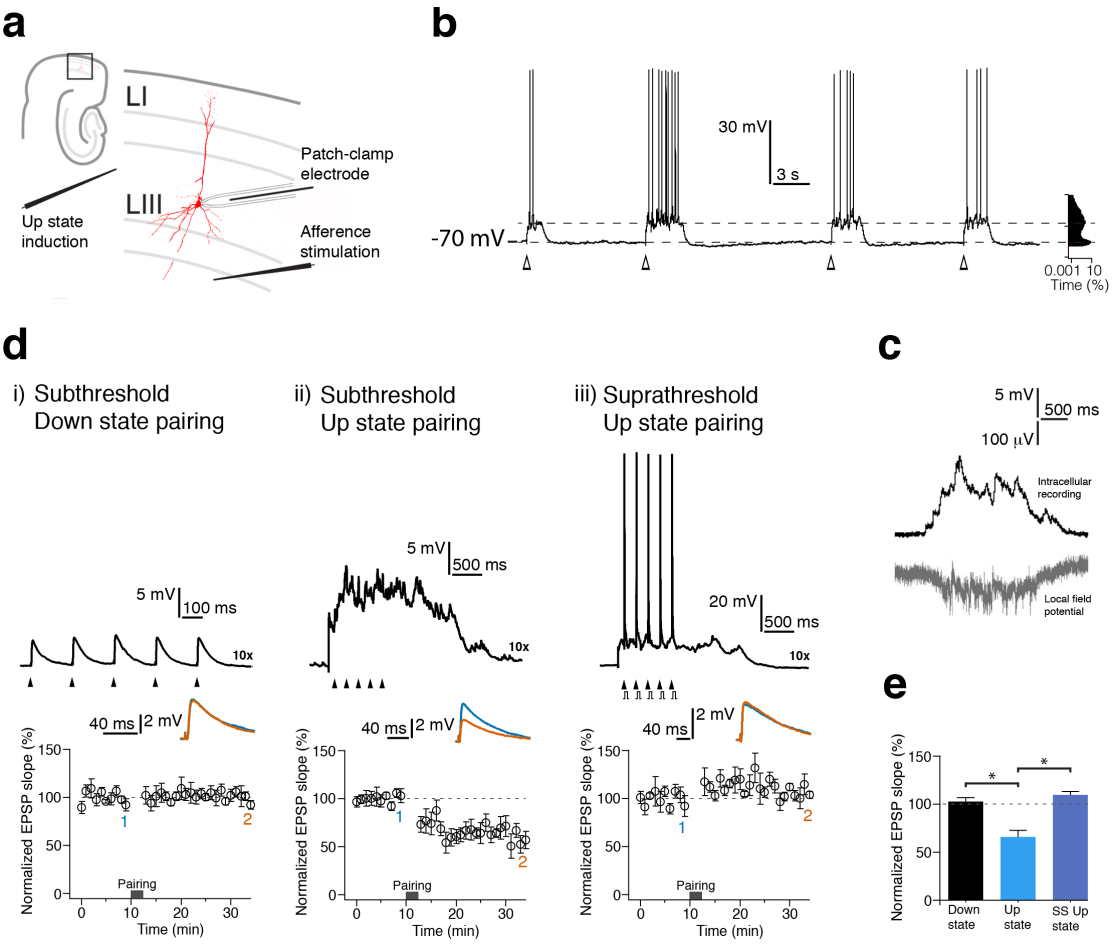

Figure 1 Pairing of subthreshold inputs with cortical Up states leads to synaptic weakening, which can be prevented by input-correlated postsynaptic Up state spiking. **(a)** Electrode placement in MEC for whole-cell patch-clamp recordings, afferent stimulation and local Up state induction. **(b)** Current clamp recording from a MEC LIII principal cell in 2 mM Ca^{2+}. Weak electrical stimulation (arrowheads) induced Up states in the recorded cell resulting in a typical bimodal distribution of the membrane potential (right histogram; percentage of time at each V_m presented on a logarithmic scale).

(c) Simultaneous local field potential (lower trace) and whole-cell patch-clamp (upper trace) recordings. **(d)** (*i)* After a ten-minute baseline recording trains of stimuli at 5 Hz (50 pairings in total) were applied for a 'Down state pairing' (upper trace, pairing average; arrowheads mark afferent stimulation), followed by EPSP measurements for at least another 20 min. The middle inset shows representative EPSPs from the baseline period (blue 1) and the end of recording (orange 2). *(ii)* Experimental conditions as in *(i)*, however, this time afferent stimulation was paired with an evoked Up state (upper trace: example pairing) (50 pairings). *(iii)* Experimental conditions as in *(ii)*, however, each afferent stimulation was followed by somatic current injection (2-12 ms after afferent stimulus) triggering one, occasionally two action potential(s) (50-100 pairings). **(e)** Summary of pairings from (d): There was a statistically significant main effect of the pairing protocol (one-way ANOVA, $F[2, 18] = 17.84$, $p < 0.0001$). A Tukey post-hoc test (significance level at 0.05) revealed that the subthreshold Up state pairing resulted in statistically significant synaptic weakening compared to the Down state pairing and suprathreshold Up state pairing, while the latter two groups were not significantly different. Error bars show the SEM.

3.3 The postsynaptic membrane potential and plasticity induction

While the specific voltage profiles at activated synapses – likely to be dendritic spines – during application of the different pairing protocols are difficult to determine, a direct comparison of our somatically recorded responses evoked by synaptic activation during baseline Down states versus pairing Up states might give at least an indication towards potential mechanisms underlying the induction of synaptic weakening. Baseline postsynaptic responses from pairing experiments in *Fig. 1d* , evoked during Down states, typically consisted of single-component EPSPs (**Fig. 2a**). The average response triggered during subthreshold Up state pairings often revealed an inhibitory component. This inhibition and a reduced driving force likely resulted in smaller (somatic) EPSP peak amplitudes (relative to the prestimulus membrane potential) during Up states in comparison to Down states (**Fig. 2b**). Nevertheless, the average EPSP peak responses from Up state pairings was clearly more depolarised compared to the baseline Down state peak response. Moreover, plotting the synaptic strength from the recording end of all subthreshold Up state pairing experiments from *Fig. 1d ii* against the average EPSP peak responses from the corresponding Up state pairings indicated a weak, yet statistically not significant correlation ($R^2 = 0.14$; p =

0.32) (**Fig. 2c**). Taken together, a role for the postsynaptic membrane potential in inducing synaptic weakening appeared possible at this stage.

Next, I performed two more control experiments further examining the mechanism underlying the induction of synaptic weakening. First, I tested if pairing of afferent stimulation with a depolarising current step, producing V_m changes that mimicked the Up state-associated depolarisation, could induce synaptic weakening (**Fig. 3**). While there was a trend towards synaptic depression and the post-pairing EPSP slope was reduced to 93.6 ± 5.6 % of the baseline value, this was not statistically significant ($p = 0.28$, $n = 6$, two-tailed t-test). Finally, in order to test whether synaptic activation needs to directly coincide with Up states for synaptic weakening to occur, the subthreshold Up state pairing protocol from *Fig. 1d ii* was slightly amended so afferent inputs were stimulated just before Up state induction (**Fig. 4**). The EPSP slope was only marginally changed to 95.8 ± 4.9 % of the baseline value ($p = 0.42$, $n = 5$, two-tailed t-test showed non-significance,).

During subthreshold pairings, stimulation of afferent inputs did not induce time-locked postsynaptic spiking, but response of the postsynaptic neuron was not controlled by current injection, and spikes between and after afferent stimuli could be observed. This raised the question as to whether unlocked spontaneous postsynaptic Up state spiking could have played a role in the induction of synaptic weakening. In five out of the nine subthreshold Up state

pairing experiments from *Fig. 1d ii* there was at least some spontaneous Up state-associated postsynaptic spiking (**Fig. 5a**). A peristimulus time histogram (spikes relative to afferent stimulation) based on those experiments from *Fig. 1d ii* with Up state spike rates > 1 Hz revealed that there was only a marginal number of spikes in typical STDP windows (**Fig. 5b**). Moreover, the average synaptic weakening of these experiments with Up state spike rates > 1 Hz (60.5 ± 13.4 %, n = 3) was similar to the average synaptic weakening of those experiments from *Fig. 1d ii* with no or little (< 1 Hz) Up state spiking during pairing (68.5 ± 24.2 %, n = 6).

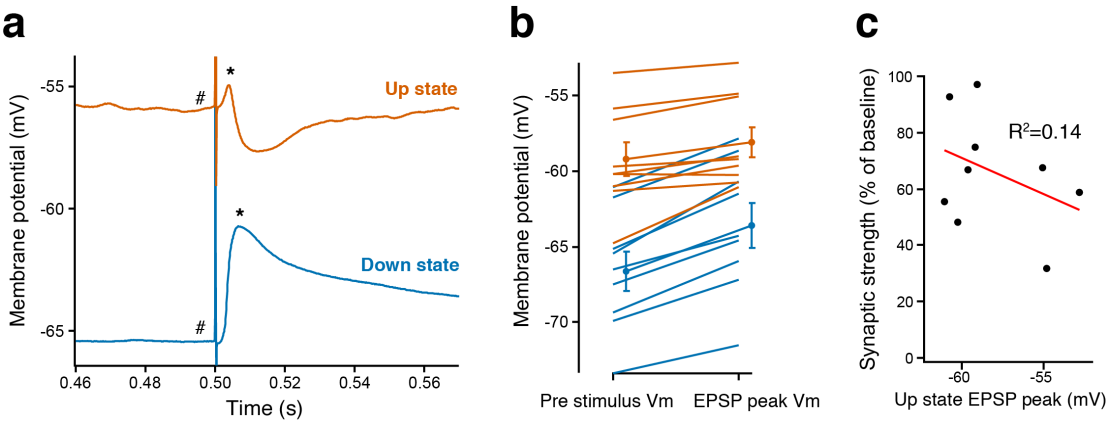

Figure 2 Comparison of postsynaptic response evoked during Down states versus Up states. **(a)** Average Down state EPSP from the baseline period (bottom trace) compared to the average postsynaptic response during the following Up state pairing (upper trace) from a representative recording from *Fig. 1d ii*. The pre-stimulus period marked with a hash (-10 ms to stimulus onset), the Down state peak response and the Up state peak response in the search window 0 – 10 ms relative to the stimulus trigger (marked with an asterisk) were determined for all Up state pairing experiments and are shown in **(b)**. Down state measurements are blue and Up state measurements are orange. **(c)** Plotting the degree of synaptic weakening from all Up state pairing experiments from *Fig. 1d ii* against the respective averaged Up state EPSP peak response shows a weak and insignificant correlation (R^2 = 0.14; p =

0.32). [Postsynaptic responses evoked during Up states that showed spiking in the relevant time period were not included in the calculation of the average response].

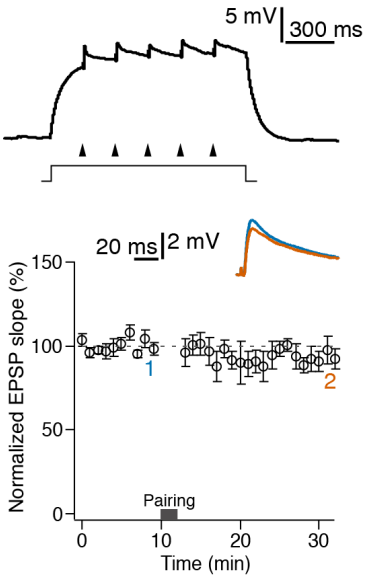

Figure 3 Pairing of afferent stimulation with induced depolarisation. Experiment in analogy to subthreshold Up state pairing experiment *Fig. 1d ii*; however, the membrane potential depolarisation associated with Up sates was approximated by a depolarising current step (induced current step amplitude: 9.3 ± 3.6 mV). It is n = 6. Error bars show the SEM.

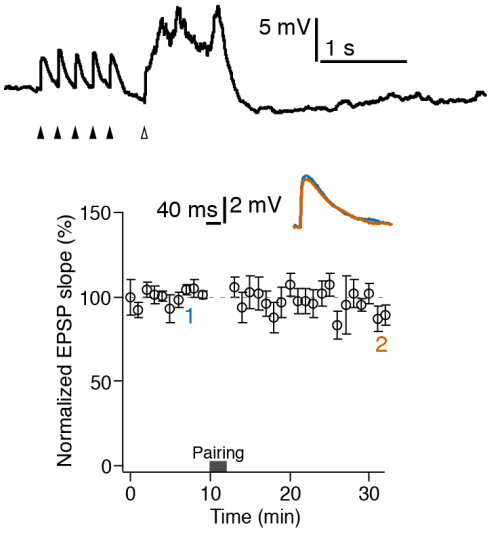

Figure 4 Pairing of afferent stimulation with a Down state (black arrowheads) followed by Up state induction (white arrowhead). It is n = 5. Error bars show the SEM.

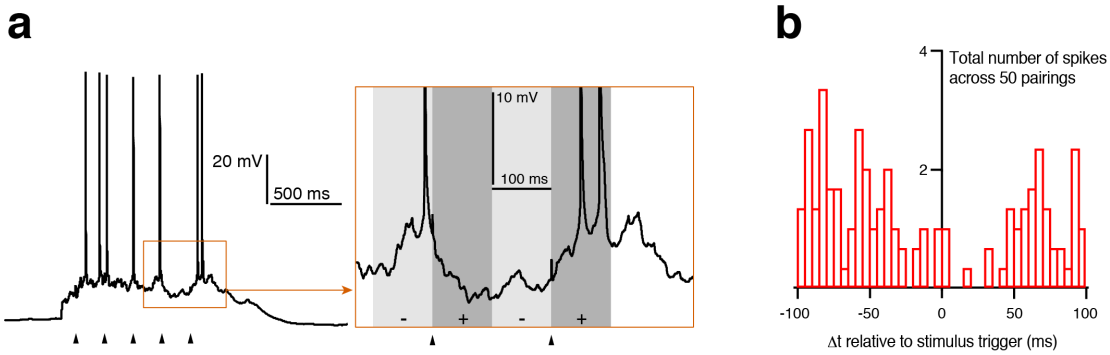

Figure 5 Up state-associated spiking in relation to afferent stimulation. **(a)** Some cells showed spontaneous Up state spiking during pairing. For each afferent stimulation (arrowheads) spikes in the preceding 100 ms and the following 99ms were determined. Shaded areas show the windows for detecting spikes before (-) and after (+) afferent stimulation. **(b)** Based on the three experiments from *Fig. 1d ii* with Up state spike rates > 1 Hz, a peristimulus spike-time histogram (PSTH) was derived: A cumulative PSTH based on all 50 pairings was calculated for each experiment; b shows the average across experiments.

3.4 De-depression of synapses by burst-STDP during Up states

In section 3.2, it was established that pairing of a postsynaptic spike with each afferent stimulation during Up states prevents synaptic weakening, and even results in a slight trend towards potentiation. Pairing of synaptic inputs with a high-frequency bursts can be particularly effective in inducing synaptic potentiation (Gustafsson et al. 1987). While I did not test such burst-LTP protocols on naive synapses, I did apply it at the end of some subthreshold Up state pairing experiments (from sections 3.2 and 4.3) that still exhibited stable recording conditions (**Fig. 6**). The representative recording in **Fig. 6a/b** and the normalised summary of the changes in synaptic strength across all

experiments in **Fig. 6c** clearly demonstrate bi-directional plasticity: The subthreshold Up state pairing resulted in reduced synaptic strength compared to the baseline value, while the application of a burst-LTP protocol with short bursts of approximately 3-4 spikes lead to an increase in synaptic strength (or a 'de-depression'). Impressively, the data indicate that the burst-LTP protocol might even result in a potentiation relative to the (original) baseline. Although more experiments will be necessary in order to test whether this is statistically significant, and whether naïve synapses can be potentiated by burst pairings, this suggests that Up states can facilitate bi-directional changes in synaptic strength.

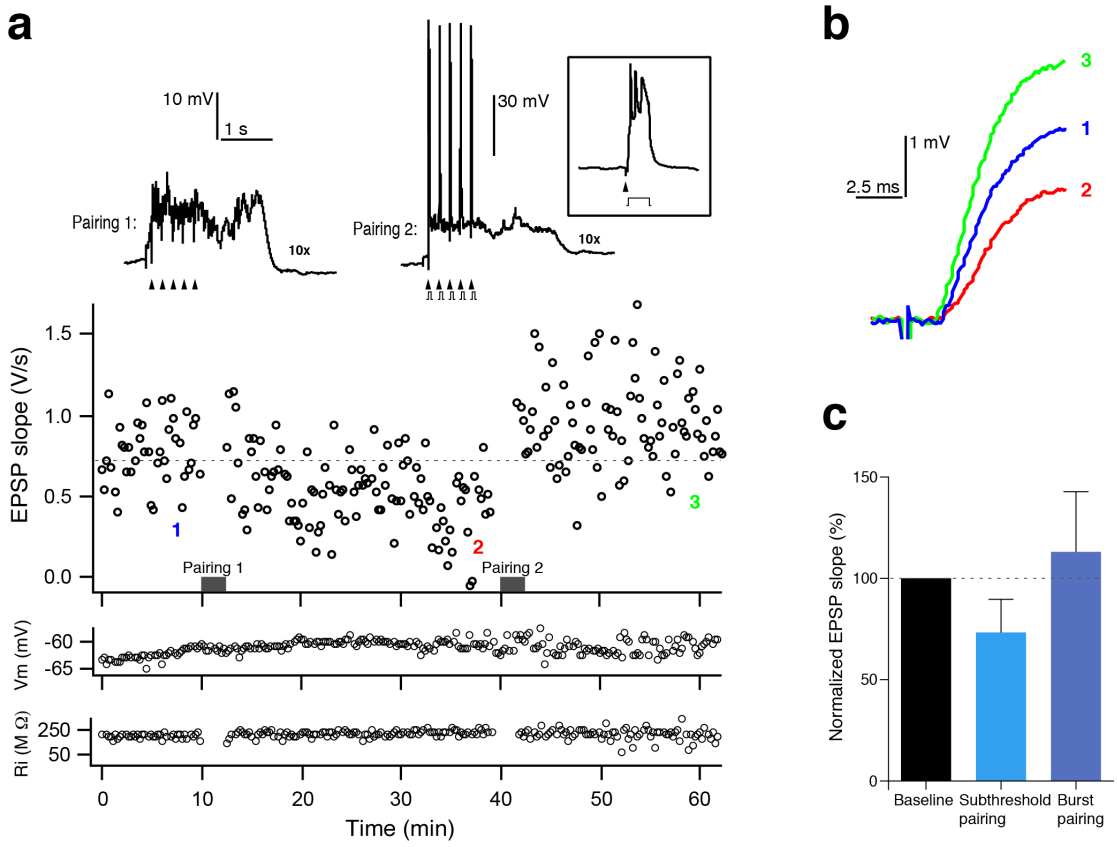

Figure 6 De-depression of synapses by burst-STDP during Up states. **(a)** Representative experiment in which, following synaptic weakening by subthreshold Up state pairings (*Pairing 1*, left trace), inputs were successfully de-depressed by another fifty input pairings with Up states (*Pairing 2*, right trace) where each input was combined with a brief current injection (2 – 22 ms after afferent stimulation, < 1 nA) that resulted in a burst of spikes in the postsynaptic cell (see inset on the right for an individual input-burst pairing). Membrane potential (V_m) and input resistance (R_i) measurements showed only marginal changes during the recording time (two bottom plots). **(b)** Representative EPSP measurements from the baseline period (blue 1), after synaptic weakening (red 2) and after de-depression (green 3) of the experiment shown in (a). **(c)** Average values (n = 3). Error bars show the SEM. [The EPSP slope measurements of the full ten minute baseline, the last ten minutes after pairing 1, and the ten minutes starting ten minutes after pairing 2 were averaged for individual *baseline*, *subthreshold pairing* and *burst pairing* experiments, respectively. All values are normalised to the baseline measurement.]

3.5 Discussion

In this chapter, I showed that pairing of synaptic inputs with Up states leads to synaptic depression or weakening of the activated connections. This synaptic weakening was prevented by input-correlated postsynaptic spiking, and it was not induced when the same stimulation protocol was applied during Down state periods. To induce synaptic weakening afferent connections were stimulated at 5 Hz. This relatively low stimulation frequency was chosen in order to avoid interactions between consecutive afferent stimulations. At this stage, however, I cannot exclude that the presynaptic cells exhibited spontaneous Up state-associated spiking during plasticity induction, which could have increased the frequency of presynaptic action potentials compared to Down state pairings. In the next chapter, I will demonstrate that natural presynaptic activity patterns can induce synaptic weakening and it is therefore unlikely that artificially high presynaptic activity patterns were essential for the induction of plasticity in the experiments discussed here.

I continued to show that evoked peak postsynaptic responses during Up state pairings were clearly more depolarised compared to peak Down state responses. Moreover, an inhibitory component in the postsynaptic response during Up state pairings was often revealed. This was likely due to the depolarisation of the postsynaptic cell revealing the presence of a disynaptic

GABA(A) receptor-mediated conductance, but could also reflect an increase in the number of inhibitory afferent fibres recruited via electrical stimulation during active network Up states (Reig et al. 2015). Additional recruitment of excitatory afferent connections during Up state pairings is also conceivable, and would constitute another possible difference to the Down state pairing group. This problem will also be addressed in the next chapter.

I observed a (admittedly very) weak correlation of evoked peak postsynaptic responses during Up state pairings and the degree of synaptic weakening, which could indicate the importance of the postsynaptic membrane potential for the induction of plasticity. This is in agreement with model predictions for the voltage-dependence of long-term depression (Clopath and Gerstner 2010).

In a previous study, LTD was induced at synapses of neocortical layer V principal cells by pairing presynaptic activity with subthreshold postsynaptic depolarisation (Sjöström, Turrigiano, and Nelson 2003). I performed a similar experiment in which depolarising current steps mimicked the Up state-associated depolarisation, but did not find a statistically significant effect on synaptic strength. This could reflect the requirement for a tightly controlled postsynaptic depolarisation for the induction of synaptic weakening that was not sufficiently approximated by somatic current injection in my experiments, and/or did not produce sufficient depolarisation in dendritic branches and

spines. Such a fine-tuned depolarisation could require coordinated inhibitory inputs as seen during Up states (Hayama et al. 2013; Neske, Patrick, and Connors 2015). A precise postsynaptic depolarisation is also at the core of STDP (Hao and Oertner 2012) and a positive single-spike t-LTP protocol has been shown to result in a relative potentiation when applied during Up states compared to Down states (Kruskal, Li, and MacLean 2013). This is consistent with my finding that positively input-correlated spikes can prevent synaptic weakening. Moreover, the strong de-depression induced by a burst-LTP protocol suggests a great flexibility in bi-directional plasticity during slow-wave activity. Such flexibility could allow a gradual synaptic depression in the course of slow-wave sleep, while at the same time allow potentiation of inputs that contributed to occasional postsynaptic bursting. Finally, I examined the role of spontaneous postsynaptic Up state spiking for the induction of synaptic weakening. Spontaneous postsynaptic spiking during pairings could contribute via spike-timing dependent synaptic depression mechanisms (Markram et al. 1997; Feldman 2000) to the observed synaptic weakening. However, cells that showed low postsynaptic spiking activity, or none at all, also underwent a reduction in synaptic strength after pairing. Moreover, in those cells with significant postsynaptic spiking, only a very small number of the total spikes directly preceded afferent stimulations, which is normally critical for the induction of t-LTD. Therefore, postsynaptic Up state spiking

appears not to be essential for the induction of synaptic weakening, and was therefore generally not controlled throughout this thesis.

4 Role of the pre- and postsynaptic cell in the induction and expression of synaptic weakening

4.1 Introduction

In the previous chapter, I identified a form of synaptic weakening that was induced by pairing subthreshold synaptic inputs with cortical Up states, with no significant changes in synaptic strength following the same pattern of afferent stimulation during Down states. Here, I attempted to characterise the locus of induction and expression of this form of synaptic plasticity in more detail.

The initial characterisation of Up state-associated synaptic plasticity used extracellular electrical stimulation in superficial MEC layer V to study the strength of synaptic inputs on to pyramidal neurons recorded in MEC layer III. This approach complicated the interpretation of mechanisms of synaptic plasticity for three key reasons - (i) the source of the afferent input could not be determined, and could include projections from layer V -> layer III (van Haeften et al. 2003; Canto, Wouterlood, and Witter 2008), collaterals of layer III projections coursing through layer V, and/or extrinsic projections to MEC, (ii) there was no control pathway to monitor any effects that were not synapse

specific – while several elements of the experimental design suggested that Up state generation per se did not lead to synaptic weakening, it was conceivable that pairing bulk afferent stimulation with network Up states could alter global parameters of synaptic transmission and/or intrinsic excitability, (iii) there was no control of spontaneous activity/excitability of the afferent fibres recruited, and thus the differences observed between Up and Down state pairings could have conceivably resulted from differences in the background spontaneous spike rates in the afferent fibres and/or differences in the set of fibres recruited. My assumption was that extracellular stimulation would preferentially activate recurrent collaterals between layer III pyramidal neurons, and the hypothesis was that plasticity at these recurrent synapses was determined by postsynaptic Up versus Down states. The first goal of this chapter was therefore to address these issues directly by performing dual whole-cell patch-clamp recordings of synaptically coupled layer III pyramidal cells, and study the rules synaptic weakening at this identified connection.

The next goal was to shine light on the molecular determinants that are necessary for the induction of synaptic weakening. The induction mechanisms for long-term depression that have been identified over the years are diverse, but many involve the temporary elevation of postsynaptic Ca^{2+} (Collingridge et al. 2010). NMDA receptors are the major source of synaptically evoked postsynaptic Ca^{2+} in dendritic spines (Higley and Sabatini 2012) and NMDAR-

dependent LTD has been identified in numerous neural circuits, including the CA1 region of the hippocampus (Dudek and Bear 1992; Mulkey and Malenka 1992), striatum (Thomas, Malenka, and Bonci 2000), visual cortex (Kirkwood and Bear 1994), perirhinal cortex (Cho et al. 2000), and entorhinal cortex (Cheong et al. 2002). Homosynaptic LTD was here induced by low-frequency stimulation of afferent fibres and, interestingly, it is often possible to augment the induction by input pairing with postsynaptic depolarisation. Thus, it is conceivable that synaptic weakening, which is induced during depolarised Up states, shares some mechanistic details with these types of LTD. However, activity-dependent forms of LTD that are independent of postsynaptic NMDA receptors could also be related to the synaptic weakening (Sjöström, Turrigiano, and Nelson 2004). In the already mentioned study by *Sjöström et al.*, fifty pairings of a presynaptic action potential with postsynaptic depolarisation induced LTD via a mechanism involving the activation of presynaptic NMDA autoreceptors and endocannabinoid receptors. Studying the role of NMDAR in synaptic plasticity during Up states is complicated by the fact that Up states themselves are blocked by NMDAR antagonists in entorhinal cortex (Dr. Ed Mann, unpublished finding). Thus, in a first attempt to reveal details of the induction mechanism of synaptic weakening, I here tested the effect of blocking NMDA receptors in the postsynaptic cell during subthreshold Up state pairings.

Wakefulness and sleep are associated with distinct gene expression profiles and molecular regulations (Cirelli 2005). The mechanism of synaptic weakening during SWA is likely to depend on some of these molecular correlates of sleep. Of particular importance here could be the glycogen synthase kinase–3β (GSK3β). GSK3β has been repeatedly linked to hippocampal synaptic plasticity and is crucial for the induction of NMDAR-dependent LTD (Peineau et al. 2007; Chew et al. 2015; Dewachter et al. 2009; Bradley et al. 2012). Interestingly, GSK3β is more active after sleep due to reduced inhibition (Vyazovskiy et al. 2008). Next, I therefore examined whether GSK3β played a role in synaptic weakening during Up states.

Finally, the plasticity data collected up to this point were analysed for indications of pre- and postsynaptic components regarding the expression of synaptic weakening. This analysis is introduced in section *4.4*.

4.2 The induction of synaptic weakening is activity-dependent and can be triggered by spontaneous presynaptic Up state spiking

I performed dual whole-cell patch-clamp recordings from synaptically coupled MEC layer III principal cells, and tested whether spontaneous presynaptic Up state spiking could induce synaptic weakening (**Fig. 7**). Out of the 108 tested pairs of principal cells 14 were identified to be synaptically connected, and only 8 paired recordings remained stable for sufficiently long to monitor synaptic plasticity. Putative synapses were found on medial sections of basal dendrites (**Fig. 7a**). Minimal injections of constant depolarising or hyperpolarising currents were used to regulate the spontaneous spiking activity in the presynaptic cell, providing two groups for Up state pairing protocols tested at monosynaptic connections between layer III pyramidal cells: Presynaptic cells in the first group showed spontaneous Up state spiking (3.4 ± 1.7 Hz, n = 4; **Fig. 7b**), while presynaptic cells in the second group did not exhibit any Up state-associated spiking activity (**Fig. 7c**). Brief current injection in the presynaptic cell every 15 s were used to evoke single presynaptic action potential and monitor the strength of the postsynaptic EPSP (**Fig. 7b/c**). After a baseline recording, Up states were evoked for 15 minutes (one per sweep). When presynaptic Up states showed spiking activity, the EPSP amplitude was reduced to 51.92 ± 10. 9 % (n = 4), while

presynaptic subthreshold Up states caused only a marginal change of the EPSP amplitude to 97.43 ± 5.7 % (n = 4). A two-tailed t-test revealed a statistically significant difference between those two groups ($p = 0.0102$). These results confirm that Up state-dependent weakening of synaptic inputs occurs at recurrent connections within MEC layer III, that Up state activity alone is not sufficient to modulate synaptic weights, and that the induction of synaptic weakening can be achieved by spontaneous presynaptic spike patterns.

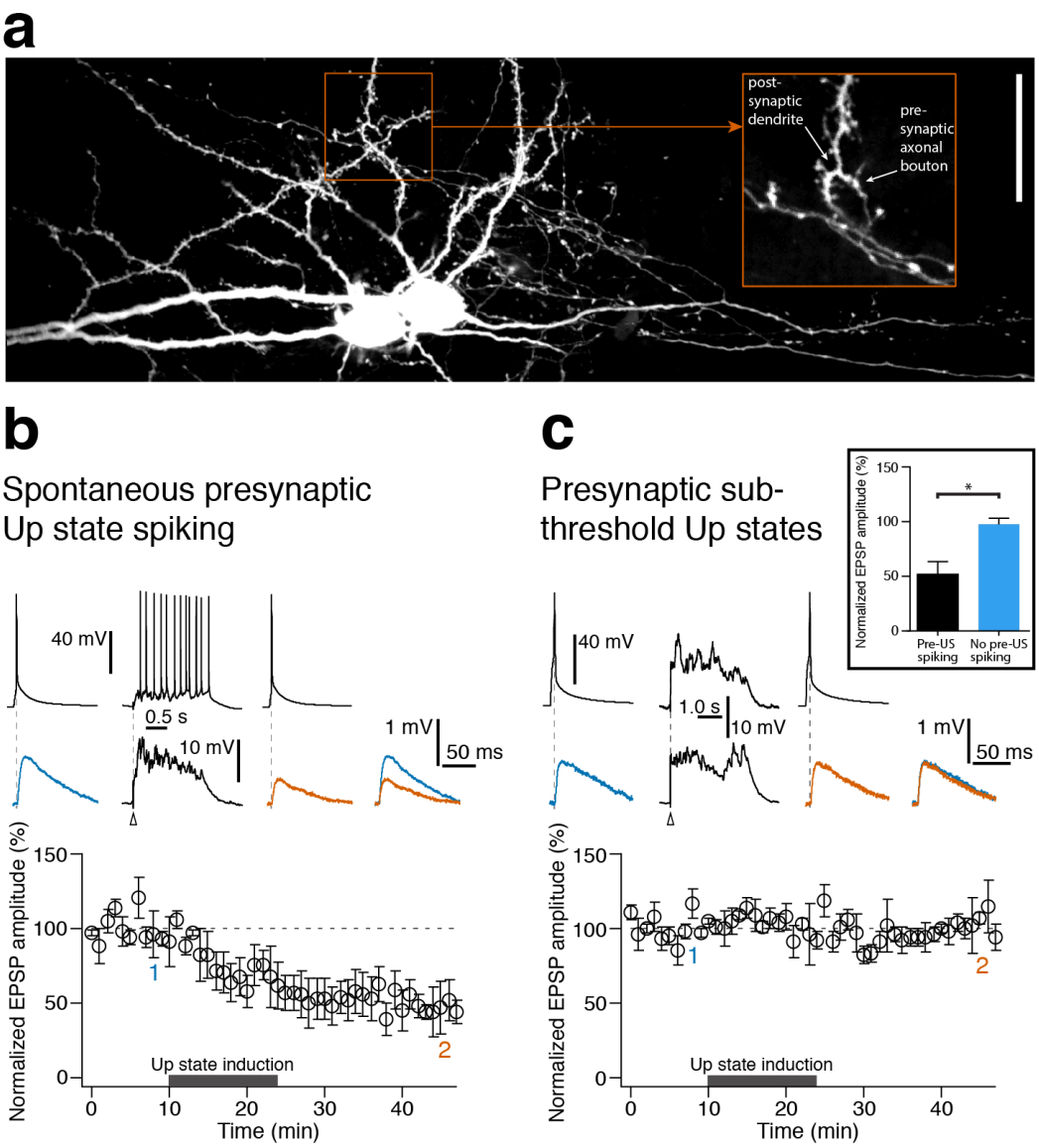

Figure 7 Synaptic weakening by spontaneous presynaptic Up state spiking. **(a)** Biocytin-labeling of two synaptically coupled MEC layer III principal cells. Inset shows a putative synapse onto a basal dendrite. Scale bar: 40 µm. **(b/c)** Dual whole-cell patch-clamp recordings from two coupled MEC layer III principal cells were established. After a ten-minute baseline Up states were evoked (arrowhead, middle traces) once every 15 s for 15 minutes. Shown are representative presynaptic action potentials and postsynaptic EPSPs from the baseline period (blue 1) and the end of recording (orange 2). Presynaptic cells in **b** showed spontaneous presynaptic Up state spiking, while presynaptic cells in **c** exhibited subthreshold Up states. Error bars show the SEM.

4.3 Postsynaptic pharmacological blockade of NMDA receptors and inhibition of GSK3β

In order to explore the mechanisms by which the postsynaptic state determines induction of Up state-mediated synaptic weakening, I first examined the contribution of postsynaptic NMDA receptors. To test this, I used the subthreshold Up state pairing protocols from *Fig. 1d ii* with two interleaved experimental groups: in the control group, as before, the patch-pipette was filled with standard internal solution, while in the second group the NMDA receptor antagonist MK-801 (200 µM) was additionally included (**Fig. 8a**). The inhibitor and control internal solution were given at least thirty minutes for equilibration after breakthrough, before recording baseline responses. Following Up state pairing, synaptic weakening to 69.34 ± 9.5 % (n = 6) in the control group was statistically significantly reduced to 94.8 ± 3.7 % (n = 6) in the inhibitor group (two-tailed t-test, $p < 0.05$).

The same intracellular pharmacology approach was used to assess the role of GSK3β in the Up state-associated synaptic plasticity. Including the GSK3β inhibitor SB415286 in the patch-pipette, at a concentration (10 µM) that had previously been reported to block LTD induced by repetitive low-frequency afferent stimulation (900 stimuli @ 1 Hz) (Peineau et al. 2007), also fully reduced synaptic weakening from 78.2 ± 3.9 % (n = 6) in the control group (vehicle in internal solution) to 104.4 ± 4.3 % (n = 6) in the inhibitor

group (**Fig. 8b**). This was again statistically significant (two-tailed t-test, $p < 0.01$).

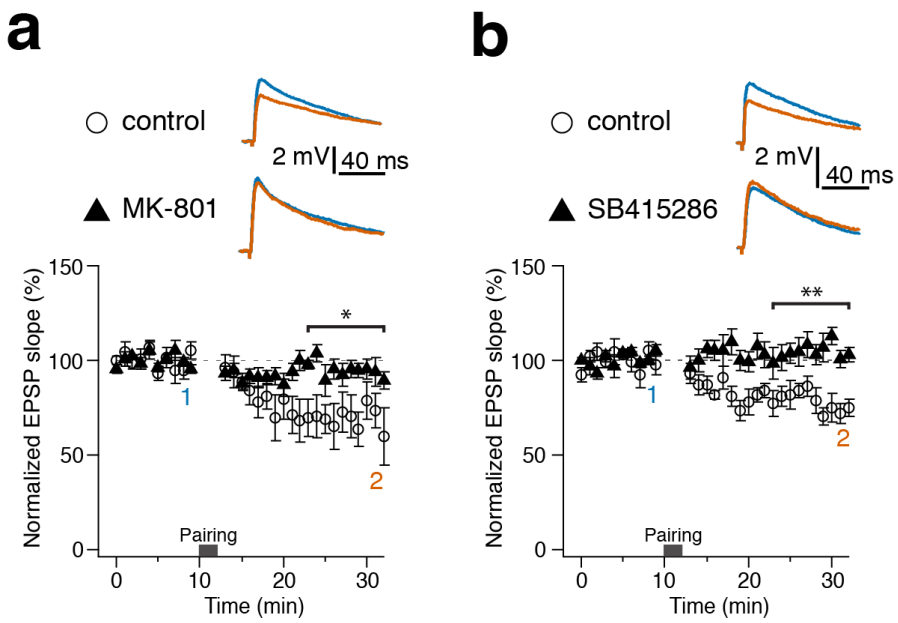

Figure 8 Role of NMDARs and GSK3β in synaptic weakening. Blocking either **(a)** NMDA receptors with MK-801 (200 µM in internal solution) or **(b)** GSK3β with SB415286 (+ 0.01 % DMSO in internal solution) reduced synaptic weakening compared to the control group (internal solution only and internal solution + 0.01 % DMSO, respectively). Error bars show the SEM.

4.4 Coefficient of variation (CV) analysis

The data from the previous section showed that molecular pathways in the postsynaptic cell involving NMDA receptors and GSK3β are critical for the induction of synaptic weakening. Next, I looked for indications towards the potential site of expression (pre- vs. postsynaptic). The most critical variables

in this context are the (glutamate) sensitivity of the postsynaptic membrane and the probability of vesicle release from the presynaptic cell (p). An easy way to determine changes in release probability p is to look for changes in the rate of synaptic transmission failures, which is what I initially attempted. Based on the four paired-recordings from *Fig. 7b* that exhibited presynaptic Up state spiking, and therefore underwent synaptic weakening, EPSP amplitude probability histograms from the baseline period and from the end of the recording were generated (**Fig. 9a**). As expected, the histograms roughly approximate a binominal distribution, and the histograms from the respective recording end displayed a left shift, reflecting synaptic weakening. However, due to the sparseness of transmission errors, and the proximity of the EPSP amplitude histogram to the distribution of the recording noise, it became quickly clear that it was impossible to extract reliable measurements of the frequency of transmission errors. Nevertheless, not one of the histograms from *Fig. 9a* indicated an increase in the failure rate – see especially *Pair 1*: the peak at approximately 0.3 mV, possibly reflecting transmission errors, did not significantly increase in the end histogram compared to the baseline histogram.

An alternative approach to investigating pre- and postsynaptic components in the expression of synaptic plasticity relies on the analysis of the coefficient of variation (CV) of the postsynaptic responses (Faber and

Korn 1991; Larkman et al. 1992; Sjöström, Turrigiano, and Nelson 2003) – an indirect method that is particularly useful when it is not possible to resolve quanta. The CV is defined as the standard deviation divided by the mean, and assuming that the data follow a binominal distribution it is:

$$(i)\quad CV = \frac{\sigma}{M} = \left[\frac{1-p}{np}\right]^{1/2} \qquad and \qquad (ii)\quad M = npq,$$

where σ is the standard deviation and M is the mean postsynaptic response within the considered time period, *p* is the probability of vesicle release from the presynaptic cell, *n* is the number of release sites and *q* is the quantal size, the postsynaptic response to the release of neurotransmitter from a single vesicle. According to *(i)* CV is independent of the quantal size, while $1/CV^2$ is directly proportional to the quantal content *np*. **Fig. 9b** shows the $1/CV^2$ values from the end phase of each of the paired-recording experiments plotted against the corresponding mean EPSP amplitude (M). Both $1/CV^2$ and M were normalised to the respective baseline value. Since CV and therefore $1/CV^2$ is independent of *q*, synaptic weakening (reflected in M < 1) that has predominantly a postsynaptic origin (reflected in changes of *q*) should result in data points close to the dotted horizontal line in *Fig. 9b,* since $1/CV^2$ should not vary. If synaptic weakening is a consequence of changes at the presynaptic site, $1/CV^2$ should decrease at least as much as M, while an origin in pre- and postsynaptic modifications should be reflected in data points

between the horizontal line and the diagonal (Faber and Korn 1991). Following this interpretation, the CV plot in *Fig. 9b* points towards a mixed expression involving the pre- and postsynaptic compartment. Because of the low number of paired-recordings, I next pooled all previous subthreshold Up state pairing experiments based on extracellular stimulation of afferent inputs (from *Fig. 1d ii* and controls from *Fig. 8)* and performed another CV analysis (**Fig. 9c**). The data seem to follow a sigmoidal curve so that data points associated with synapses that only display a low degree of synaptic weakening (normalised values of M close to 1) lie near the horizontal line, while data points associated with more strongly depressed synapses lie under the diagonal. The former is consistent with a postsynaptic or mixed pre- and postsynaptic origin of plasticity, while the latter indicates predominant changes in the presynaptic cell (e.g. release probability).

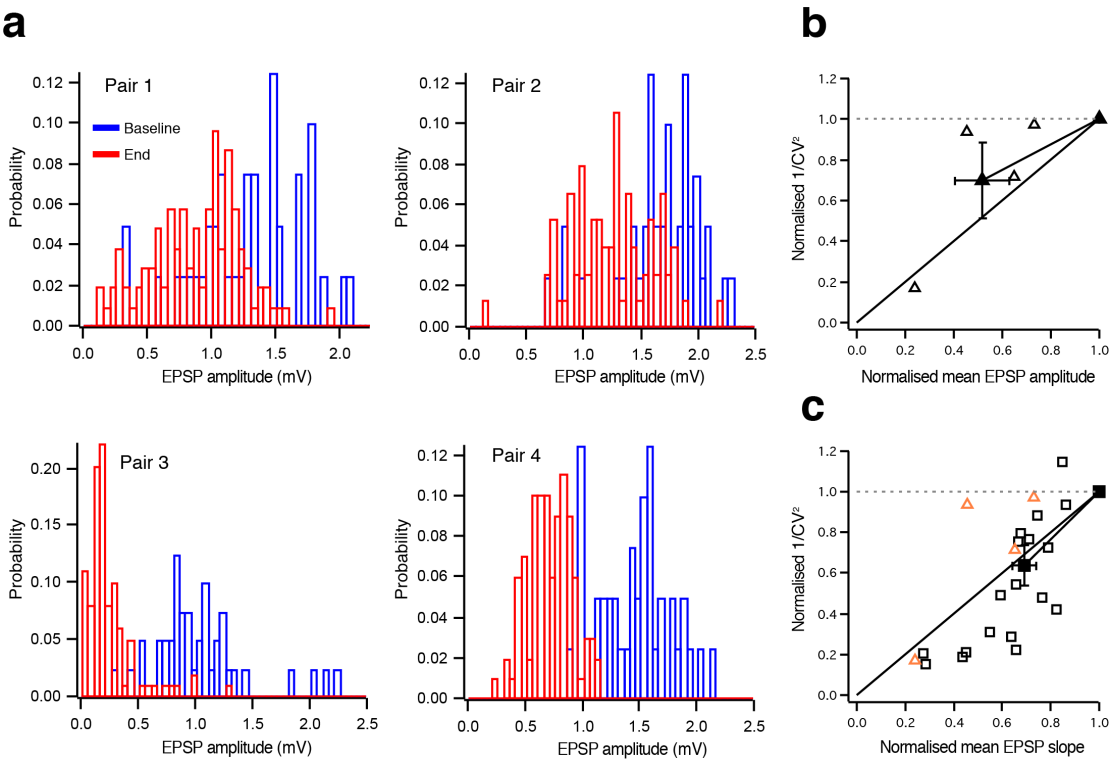

Figure 9 Pre- and postsynaptic expression of synaptic weakening. **(a)** EPSP amplitude probability histograms for the four paired-recordings from *Fig. 7* with presynaptic Up state spiking. Shown are histograms from the baseline period (blue) and the end of the respective recording (red). **(b)** CV analysis for the four pairs with presynaptic Up state spiking. The $1/CV^2$ value based on the EPSP amplitude measurements from the end of the respective recording was normalised to the $1/CV^2$ value from the baseline period. In the same way, the mean EPSP amplitude from the end of the recording was normalised to the respective baseline mean. **(c)** CV analysis based on all subthreshold Up state pairing experiments that showed synaptic weakening (black rectangles; n = 19). Measurements from b are also shown (orange triangles) for comparison. EPSP measurements from the last five-minute interval of the baseline were used to calculate baseline mean and CV, while EPSP measurements from the five-minute interval starting fifteen minutes after the Up state pairing were used to calculate mean and CV after plasticity induction. Noise corrections had minimal effects on the analysis and were omitted. Error bars show the SEM.

4.5 Discussion

In this chapter, more detailed mechanistic aspects of synaptic weakening were examined. First, it was found that synaptic weakening also exists in local circuits at identified LIII-LIII connections of principal cells. Here, induction was achieved by spontaneous presynaptic spiking during Up states, while there was no obvious change in synaptic strength when the presynaptic cell did not spike during Up states. Assuming that synaptic weakening occurs in the entire dendritic tree, these results indicate that synaptic weakening is relatively input-specific. However, it needs to be pointed out that, due to the difficult technical nature of the experiments, these findings are based on a very small number of recordings and supportive experiments should be conducted in the future. Furthermore, another set of paired-recording experiments needs to be carried-out, in which spontaneous presynaptic Up state spiking is suppressed and instead presynaptic spikes are triggered at 5 Hz in analogy to the subthreshold Up state pairing experiments from chapter 3. This will show whether the characteristics of spontaneous presynaptic Up state spiking (e.g. frequency or more specific temporal spiking dynamics) are crucial for the induction of synaptic weakening. At this stage, I would suggest that neither background firing rates in presynaptic fibres, nor the coordinated patterns of presynaptic spiking, are essential for inducing Up state-associated plasticity:

in the subthreshold Up state pairing experiments from chapter 3, induction of synaptic weakening was very reliable, and yet neither of these parameters was under control. Since there is a relatively high chance that some of the afferent axons were cut due to the slice preparation, these connections would not have had spontaneous spiking activity.

I showed that postsynaptic blockade of NMDA receptors or the inhibition of GSK3β blocked the induction of synaptic weakening. In these experiments, the pharmacological agents were included in the patch-pipette and they were thus present throughout the recording and could also have affected the maintenance phase of synaptic weakening. However, both NMDA receptors and GSK3β have previously been found to participate in the induction of certain forms of LTD (Kemp and Bashir 2001; Peineau et al. 2007) and it appears likely that this is also their primary role in synaptic weakening.

Following the successful postsynaptic induction of synaptic weakening, what is the site of expression? The CV analysis performed here is consistent with a varying locus of expression depending on the degree of synaptic plasticity: a low degree seems to be mostly postsynaptically expressed, while strong synaptic weakening is dominated by a presynaptic component. Such a differential expression would be an intriguing mechanism; however, the CV analysis is prone to misinterpretation if there is a contribution of unexpected physiological variances. Particularly relevant in this context are intrinsic

parameter variances and problems that can arise when multiple afferent connections are stimulated, both of which could lead to the misidentification of a pre- or postsynaptic component (Faber and Korn 1991). Although I used the minimal stimulation strength to activate afferent inputs by extracellular stimulation, it is possible that multiple afferent axons where stimulated. Based on such experimental conditions, *Faber and Korn* constructed several theoretical scenarios where uneven synaptic plasticity across multiple stimulated axons could, for example, lead to an identification of a presynatpic component, although synaptic depression is exclusively expressed in the postsynatpic cell. Therefore, the CV analyses performed here should be considered inspiration for future working hypotheses on the mechanisms of expression of synaptic weakening, rather than strong evidence in any direction. Now assuming that a varying locus of expression indicated by the CV analysis is in fact true. How could the results of this chapter in conjunction with knowledge of mechanisms of LTD from previous studies account for such findings? The dependence on postsynaptic NMDAR and GSK3β for induction of synaptic weakening indicates mechanistic similarities with NMDAR-dependent LTD. This type of LTD is probably predominantly expressed in the postsynaptic cell via, for example, changes in AMPA receptor availability and function (Collingridge et al. 2010). However, NMDAR-dependent LTD often requires several hundred low-frequency afferent stimulations to achieve

significant depression (e.g. Cheong et al. 2002), while synaptic weakening could be induced with very few stimuli applied over a relatively short time period. As previously discussed, synaptic weakening has also some striking similarities with a type of cortical LTD that is presynaptically expressed and independent of postsynaptic NMDA receptors (Sjöström, Turrigiano, and Nelson 2004). In an attempt to reconcile all these findings, it is conceivable that two separate mechanisms of synaptic depression can be induced by subthreshold Up state pairings: a low degree of synaptic weakening is predominately mediated via a mechanism related to NMDAR-dependent LTD, while stronger synaptic weakening additionally or predominantly induces presynaptic changes. In agreement with this hypothesis, *(1)* the degree of synaptic weakening in the control group of the MK-801 experiments (*Fig. 8a*) was relatively low, and *(2)* MK-801 might not have fully blocked synaptic weakening (see inhibitor group in *Fig. 8a*). The latter could be due to the relatively low concentration of MK-801 used here (see *Methods* section) or it could be the result of synaptic weakening that did not dependent on postsynaptic NMDA receptors and was presynaptically expressed. Further supporting evidence can be found in previous LTD studies: NMDAR-dependent LTD is typically induced with single-pulse (or 'single-shock') LFS, while presynaptically expressed LTD often required paired-pulse LFS (Massey and Bashir 2007). The latter could reflect the need for an increased

depolarisation during plasticity induction. Interestingly, I found in chapter 3 a weak correlation between the degree of synaptic weakening and the postsynaptic depolarisation during plasticity induction (*Fig. 2c*). Therefore, it may be that during the induction of both paired-pulse LFS and during subthreshold Up state pairings that later resulted in strong synaptic weakening the postsynaptic cell was sufficiently strong depolarised to trigger presynaptic changes.

Future experiments investigating synaptic weakening during interference with potential retrograde signalling such as cannabinoid signalling (Sjöström, Turrigiano, and Nelson 2003; Sjöström, Turrigiano, and Nelson 2004) will have to clarify this.

5 Imaging neural activity during Up-Down state oscillations

5.1 Introduction

Excitatory afferents innervating cortical pyramidal neurons preferentially terminate on dendritic spines. These postsynaptic specialisations usually possess a bulbous spine head, connected to the parent dendrite by a thin spine neck. The presence of spines thus serves to increase the postsynaptic area of each cortical pyramidal neuron, and maximise the capacity for synaptic connections. The thin neck also creates a chemical and electrical compartment, with unique properties for signal integration that shape the rules of synaptic plasticity (Sabatini, Maravall, and Svoboda 2001; Hao and Oertner 2012). Ca^{2+} signalling in the spine head is here of particular importance: increases in spine Ca^{2+} via glutamate receptors (NMDARs, Ca^{2+}-permeable AMPARs), voltage-gated Ca^{2+} channels and release from internal Ca^{2+} stores (Higley and Sabatini 2012), have all been linked to the induction of LTD (Massey and Bashir 2007; Collingridge et al. 2010). In the previous chapter, I demonstrated that NMDA receptors also contribute to the induction of synaptic weakening during Up states. Similarly, GSK3β is necessary for the induction

of synaptic weakening, and is a kinase that is regulated by intracellular Ca^{2+} pathways (Bradley et al. 2012). The goal of the experiments in this chapter was to further clarify the role of Ca^{2+} signalling in the induction of synaptic weakening.

It has been suggested that characteristics of postsynaptic Ca^{2+} transients are directly related to the sign of synaptic plasticity: in this model, low postsynaptic Ca^{2+} elevations cause no change in synaptic weight, moderate and slow Ca^{2+} transients cause depression, while large Ca^{2+} elevations result in potentiation (Lisman 1989; Artola and Singer 1993). Considering a unified model of synaptic plasticity that has postsynaptic depolarisation at its core (Clopath and Gerstner 2010), this association between membrane potential, Ca^{2+} influx and synaptic plasticity could be explained simply by the voltage-dependence of NMDAR-mediated Ca^{2+} currents (Hao and Oertner 2012). Further support comes from several experimental studies. For example, using Ca^{2+} uncaging, LTD or LTP was selectively induced by Ca^{2+} transients that had the appropriate characteristics as mentioned above (Yang, Tang, and Zucker 1999). Moreover, in a t-LTD protocol that required localised GABAergic inhibition to supress dendritic Ca^{2+} transients, a low but not high concentration of a Ca^{2+} chelating agent could substitute for active inhibition (Hayama et al. 2013). In contrast, in spines of basal dendrites of neocortical layer 2/3 principal cells, the peak Ca^{2+} elevation during the induction of

plasticity was related to the (absolute) magnitude of synaptic plasticity, but the same peak Ca^{2+} elevation could cause either LTP or LTD (Nevian and Sakmann 2006). Furthermore, it was suggested that the exact spatiotemporal dynamics rather than the magnitude of Ca^{2+} signals alone is crucial in determining the sign of plasticity (Wang et al. 2005). It is therefore still an unresolved issue how exactly the postsynaptic Ca^{2+} signals relate to the induction of plasticity, and the existence of several distinct mechanisms seems likely.

Resolving the mechanistic details underlying synaptic plasticity will thus require direct recordings of neural activity in dendrites and spines, including postsynaptic membrane potential and intracellular Ca^{2+} dynamics (Peterka, Takahashi, and Yuste 2011; Grienberger and Konnerth 2012). Small dendritic compartments (such as basal dendrites) are largely inaccessible to electrophysiological recordings, but can be targeted using optical imaging techniques. Moreover, nonlinear microscopy offers sufficient spatial resolution for the investigation of activity in individual dendritic spines.

Thus, to shine light on the role of Ca^{2+} in the induction of synaptic weakening, I directly compared the spine head Ca^{2+} transients evoked in the same spine during consecutive Up states versus Down, using multi-photon microscopy (*5.2*). Finally, as a first step in studying spontaneous spine Ca^{2+} signalling during Up states, the temporal profile of spontaneous spine

activations across the Up state period was determined (*5.3*). In the sections below, I introduce a novel type of multi-photon microscope that was used for these experiments.

5.1.1 Fast three-dimensional multiphoton imaging utilising remote-focusing microscopy

A substantial part of my first DPhil year was spent setting up a system for simultaneous two-photon imaging and whole-cell patch-clamp recordings (**Fig. 10a**). This imaging system was based on the remote-focusing technology, which enables high-speed 3-dimensional scanning of a diffraction-limited focal spot along arbitrary trajectories (Botcherby et al. 2007; Botcherby et al. 2012). Scan-paths were defined based on a 3D image stack encompassing the target segment of the dendritic tree (**Fig. 10b**). These trajectories were usually circular and covered several spine heads and the adjacent dendritic shaft. Although scanning of only short dendritic segments was necessary within the scope of this thesis, in the future, this technology will allow the quasi-simultaneous Ca^{2+} imaging of entire dendrites and thus promises new insights into the spatiotemporal dynamics of dendritic activity.

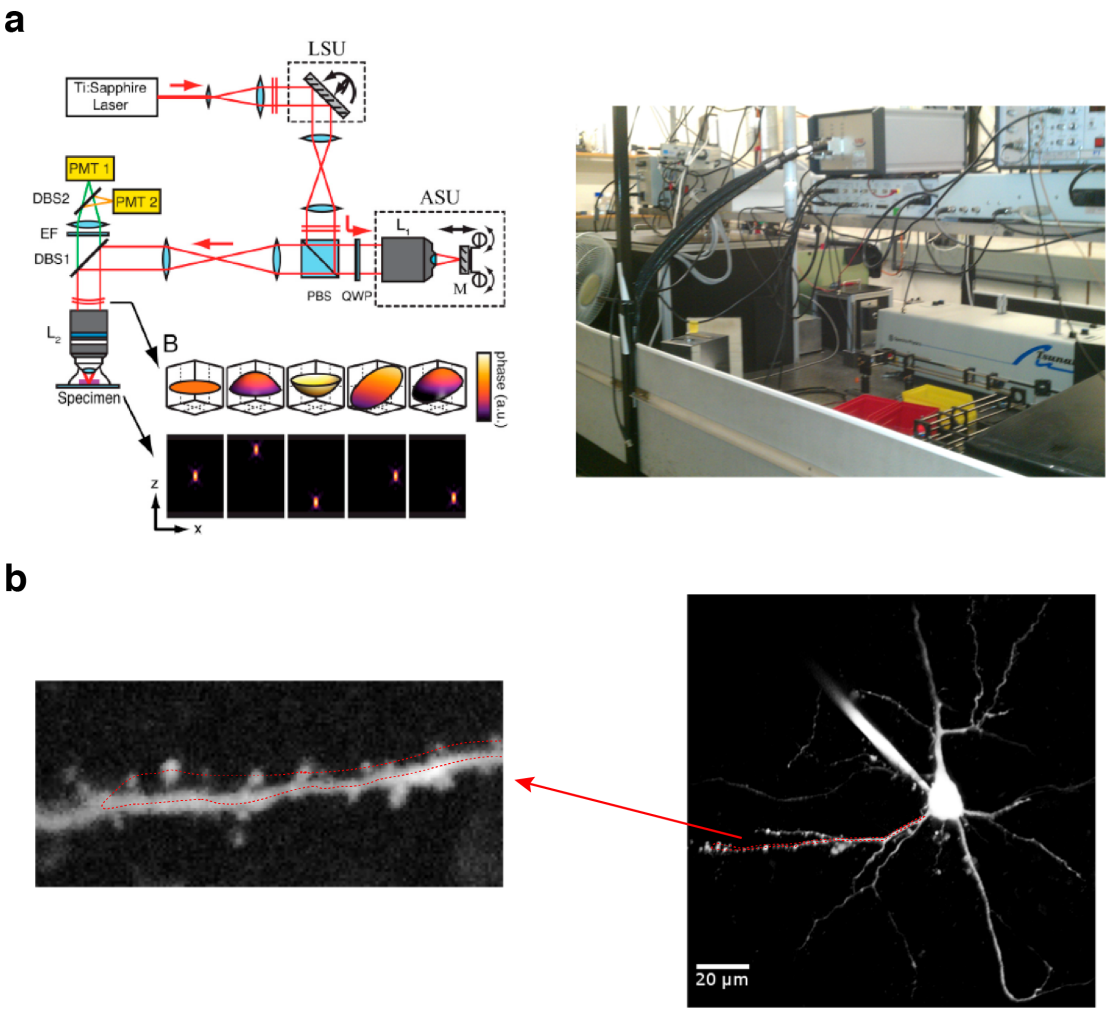

Figure 10 Ultrafast 3D calcium imaging using the remote-focusing technology. **(a)** Schematic layout of the remote-focusing microscope. Lateral and axial scan mirrors produce changes in tilt and defocus of the illumination wavefront, moving a diffraction-limited spot to any point in the specimen volume. **(b)** Z-projection of a 3D image stack of a MEC layer III principal cells filled with Alexa 594 (40 µM). This image stack was used to define an arbitrary scan-path; here, through some spine heads and the adjacent shaft of a basal dendrite (red dotted line). Note that the scan-path was also Z-projected for visualisation, but actually constitutes a trajectory within 3D space.

5.1.2 Second-Harmonic Generation (SHG) imaging of neurons – a promising, but immature technology

Imaging of Ca^{2+} has provided a wealth of important insights into intracellular signalling of neurons, but Ca^{2+} transients are slow and no substitute for measurements of the membrane potential. One- or two-photon fluorescence measurements of voltage-sensitive dyes (VSD) allow the optical measurements of fast changes in the local membrane potential of small neuronal compartments (Peterka, Takahashi, and Yuste 2011). However, fluorescence generated by dye molecules in the cytosol that are not directly influenced by the membrane voltage contaminate the signal and make quantifications in terms of absolute voltage changes difficult. Imaging based on second-harmonic generation (SHG) signals, also a non-linear optical process, has recently emerged as an alternative to two-photon VSD imaging. It solves the problem of signal contamination by free dye molecules in the cytosol, because SHG is only generated under certain environmental conditions that happen to be only given when dye molecules are aligned in the cell membrane (Campagnola et al. 1999). Therefore, absolute voltage changes can be determined after calibration. SHG imaging in neurons at subcellular resolution has only been successfully demonstrated in a few pilot studies (Dombeck et al. 2005; Rama, Vetrivel, and Semyanov 2010) and I attempted to establish this technology in combination with remote-focusing

imaging. For this, I loaded neurons deep within the tissue with the dye FM4-64 (**Fig. 11**). Indeed, I was able to measure SHG signals from these cells. As illustrated in *Fig. 11*, the SHG signal had to be collected under the condenser by the photomultiplier tube (PMT) 1 because the emission of photons by the SHG process is directed, as opposed to the simultaneously generated two-photon excitation fluorescence (TPEF) signal, which is emitted in random directions and could be collected 'behind' the imaging objective with the PMT 2. A direct comparison of the SHG image with the TPEF image demonstrates much less background contamination in the former. Beyond these proof-of-principle experiments, however, I was not able to measure changes in the SHG signal as I experienced frequent problems with phototoxicity. Such photodamage appears to be the main limitation for SHG imaging with currently available dyes (Sacconi, Dombeck, and Webb 2006). Thus, SHG is a promising new imaging approach for the determination of absolute voltage changes in dendritic compartments that could dramatically increase our understanding of the mechanisms underlying synaptic plasticity. However, the success will likely dependent on the development of new dye generations.

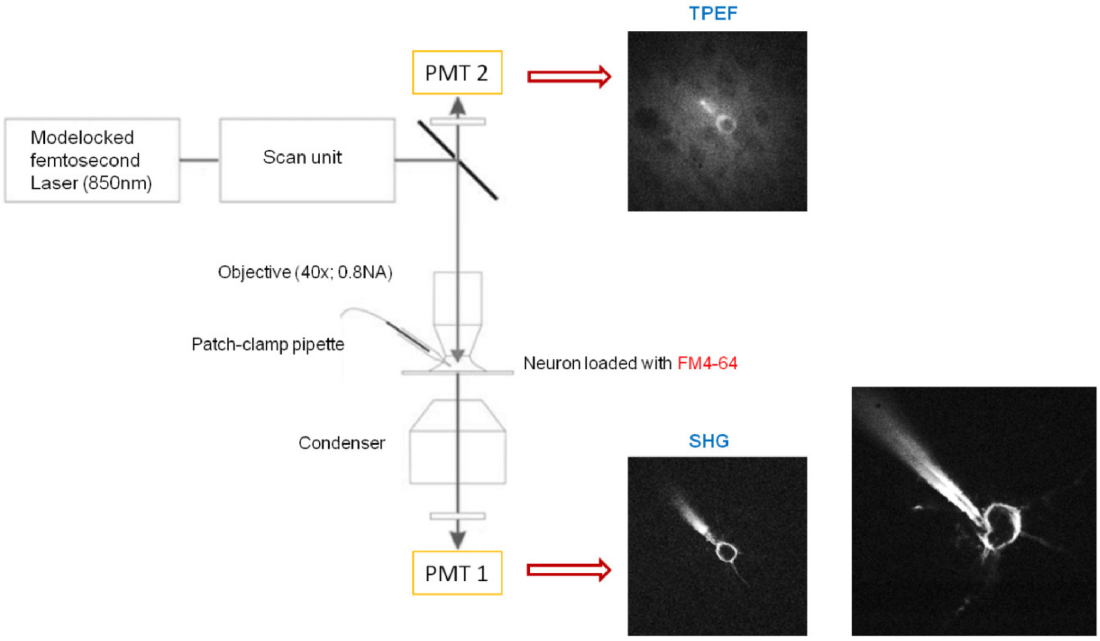

Figure 11 SHG signals from neurons located deep in acute-slice preparations. Shown is a schematic of the experimental set-up. Cortical neurons were loaded via a patch-pipette with the dye FM4-64 (200 µM in patch pipette). I was able to detect the forward-directed SHG signal in the PMT 1 and simultaneously acquired a two-photon excitation fluorescence (TPEF) image via photomultiplier 2. As expected, the SHG signal seems to be restricted to the plasma membrane.

5.2 Boost of basal spine Ca^{2+} during Up states relative to Down states

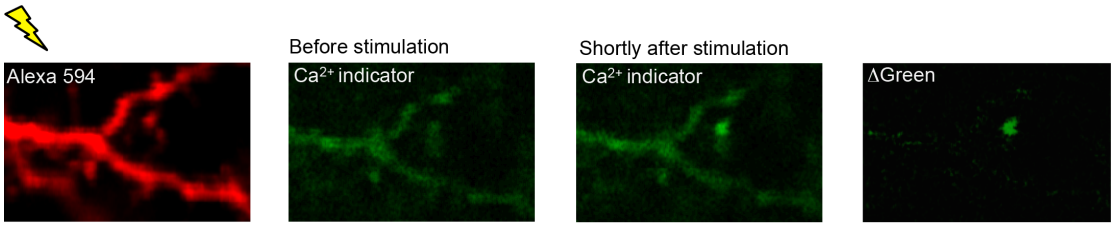

Figure 12 Synaptic activation of spines by local electrical stimulation. The structural dye Alexa 594 allowed the identification of dendritic spines (left panel) within the basal dendritic tree. Local electrical stimulation led to the activation of single (or very few) adjacent spines, which was evident by increases in fluorescence of the Ca^{2+}

indicator being restricted to one spine head in the field of view (see the 'after - before' subtracted image on the right).

As discussed in detail further above, a rise in the Ca^{2+} concentration in dendritic spines is often linked to the induction of synaptic plasticity. Ca^{2+} entry through NMDA receptors is here of particular importance and it is strongly modulated by the postsynaptic membrane potential (Higley and Sabatini 2012; Hao and Oertner 2012; Seong, Behnia, and Carter 2014). Thus, cortical slow-wave activity, which is the result of the synchronised fluctuation of the membrane potential of cortical neurons between Up states and Down states, could facilitate the generation of unique Ca^{2+} signatures at activated spines depending on the slow-wave phase. Such distinct Ca^{2+} signatures could drive different plasticity processes. However, the impact of cortical Up states on spine Ca^{2+} transients is particularly difficult to predict. Cortical Up states are the result of complex, dynamic compositions of excitatory and inhibitory conductances (Sanchez-Vives and McCormick 2000; Shu et al. 2006), which could lead to distinct spatiotemporal voltage profiles within dendrites. Furthermore, spine-targeting interneurons co-active during Up states could selectively suppress Ca^{2+} signals (Higley 2014).

To investigate the effect of the slow-wave phase (Up state vs. Down state) on spine Ca^{2+} transients, I combined two-photon spine Ca^{2+} imaging with local electrical activation of synapses. MEC layer III principal cells were

loaded with the calcium indicator Fluo-5F (400 µM) and Alexa 594 (40 µM) for at least thirty minutes via a patch-pipette. Another microelectrode filled with Alexa Fluor 594 was positioned near a basal dendrite (approximately 5 - 20 µm distance to imaged spine) for local synaptic activation (**Fig. 12** and **Fig. 13a**). I targeted dendritic locations where I had previously observed LIII-LIII synapses (see *Fig 7a*). Cells were minimally hyperpolarised to minimise Up state spiking, and prevent contamination of the recorded postsynaptic Ca^{2+} transients by back-propagating action potentials. As expected, local synaptic stimulation during Down states resulted in EPSPs and Ca^{2+} transients in the spine head, while the adjacent dendritic shaft showed only a marginal change in fluorescence (left, **Fig. 13b**). Synaptic activation of the same input during Up states produced a smaller change in the somatic membrane potential, but also reliably evoked Ca^{2+} responses that were mostly restricted to the spine head (middle). A spontaneous Up state-associated spike burst resulted in large Ca^{2+} transients in the shaft and spine head (right), confirming that Ca^{2+} signals could be detected in both compartments. In order to directly compare Ca^{2+} responses evoked during the respective phase of the slow oscillation, synaptic activation was alternately triggered during a Down state followed by an Up state period, and the mean signals evoked during successful synaptic transmissions were then compared (**Fig. 13c**). The average Ca^{2+} response evoked during Up states (46.6 ± 7.4 % ΔF/F) was consistently and

significantly increased compared to the average Down state response (31.4 ± 4.6 % ΔF/F; n = 5, $p < 0.05$, paired t-test). [In two further experiments in analogy to *Fig. 13,* Fluo-5F was replaced with the Ca^{2+} indicator OGB-1 (200 µM). The data followed a similar trend (not shown here).] Thus, synaptically activated dendritic spines have information about the network state encoded in their (mean) Ca^{2+} response during the cortical slow oscillation.

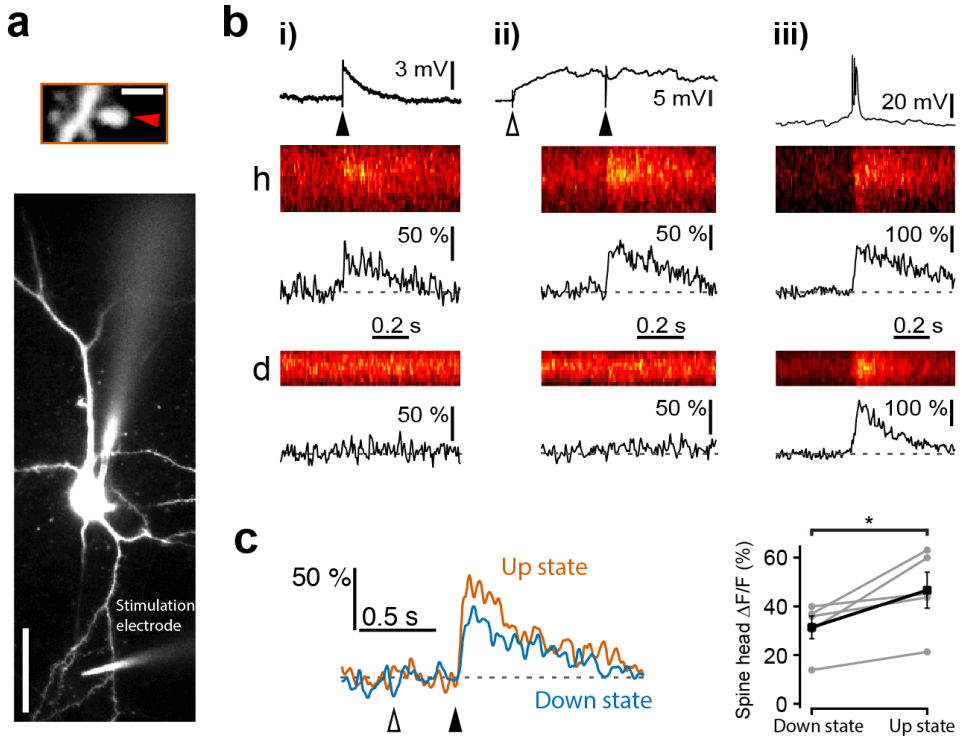

Figure 13 Increase in synaptically-evoked Ca^{2+} transients during Up states. **(a)** Experimental setup for two-photon spine Ca^{2+} imaging, local synaptic activation and Up state induction (stimulation electrode for the latter not in the field of view). The inset above shows the dendritic spine that was imaged in b. The cell was loaded with Alexa 594 (40 µM) and Fluo-5F (400 µM) for structural and Ca^{2+} imaging, respectively. Scale bars: 2.5 µm / 40 µm. **(b)** Somatic voltage responses (top traces), and corresponding relative changes in Fluo-5F fluorescence (ΔF/F) in the spine head (h; middle traces) and adjacent dendritic shaft (d; bottom traces) evoked by (i) local synaptic stimulation during Down states, (ii) local synaptic stimulation during Up states, and (iii) a spontaneous burst of action potentials during an Up state. ΔF/F is displayed as both line-scans, and the mean temporal profile across the scanning window, with panels i and ii representing the mean of three responses. **(c)** Mean spine ΔF/F responses evoked during alternating Down states (blue) and Up states (orange) from a representative recording (left). Black arrowhead marks time of synaptic stimulation, and white arrowhead marks time of Up state induction (orange Up state trace only). Comparison of the mean spine ΔF/F responses (400 ms window) evoked by local synaptic stimulation in Down states vs Up states across different neurons, with quantification based on raw traces (n = 5; right). Error bars show the SEM. Details of Ca^{2+} response filtering provided in Methods section.

5.3 Temporal dynamics of spontaneous Up state-associated spine Ca^{2+} transients in basal dendrites

Recent studies have described anatomical (McBride et al. 2008) and functional clustering (Kleindienst et al. 2011; Takahashi et al. 2012) of synaptic inputs onto the dendritic tree inspiring 'clustered plasticity models' of memory, in which synaptic clusters are key computational and storage elements. When a dendritic spine is activated during an Up state the activity of its direct neighbour spines could similarly have a particularly strong cooperative effect on the response and, for example, influence the magnitude of the spine Ca^{2+} boost described in the previous section (see Harnett et al. 2012 for an examination into the influence of synaptic cooperativity on NMDAR-dependent Ca^{2+} transients). As a first step in studying the dynamics of spontaneous spine Ca^{2+} transients during Up states, I examined when individual spines in basal dendrites are activated relative to Up state onset (**Fig. 14**). Again, MEC layer III principal cells were loaded with the calcium indicator Fluo-5F (400 μM) and Alexa 594 (40 μM) for at least thirty minutes via a patch-pipette and scan paths through basal spines were defined (as before, in medial dendritic sections; **Fig. 14a**). Several Up states were triggered with approximately 10-15 s delays, while changes in Fluo-5F fluorescence in spine heads were imaged (**Fig. 14b**). Cells showed temporally

dispersed responses throughout the Up state period, with consecutive Up states often eliciting Ca^{2+} responses with very different latencies (see responses 1 and 2). Some traces showed a plateau phase (see response 3), possibly the consequence of an extended burst of presynaptic action potentials, while some Up states did not evoke a response at all in a spine that was previously active (response 4). That this lack of a response was not due to bleaching of the Ca^{2+} indicator is evident by the later recorded spine Ca^{2+} response associated with a back-propagating action potential (see 5). Next, in order to generate a more quantitative representation of the spine activation profile, the onset latencies of the spine Ca^{2+} transients were determined in relation to Up state onset and normalised to the Up state duration (see upper panel in **Fig. 14c** and also **Methods** section). An onset latency probability histogram based on all measured Ca^{2+} responses was generated (**Fig. 14c).** Although it needs to be said that the dataset underlying this plot is very limited (14 spine Ca^{2+} transients from 3 cells from 3 mice), it indicates that, at least in medial entorhinal cortex, neurons receive excitatory inputs relatively uniformly distributed across the Up state period (from afferent inputs that form synapses with spines).

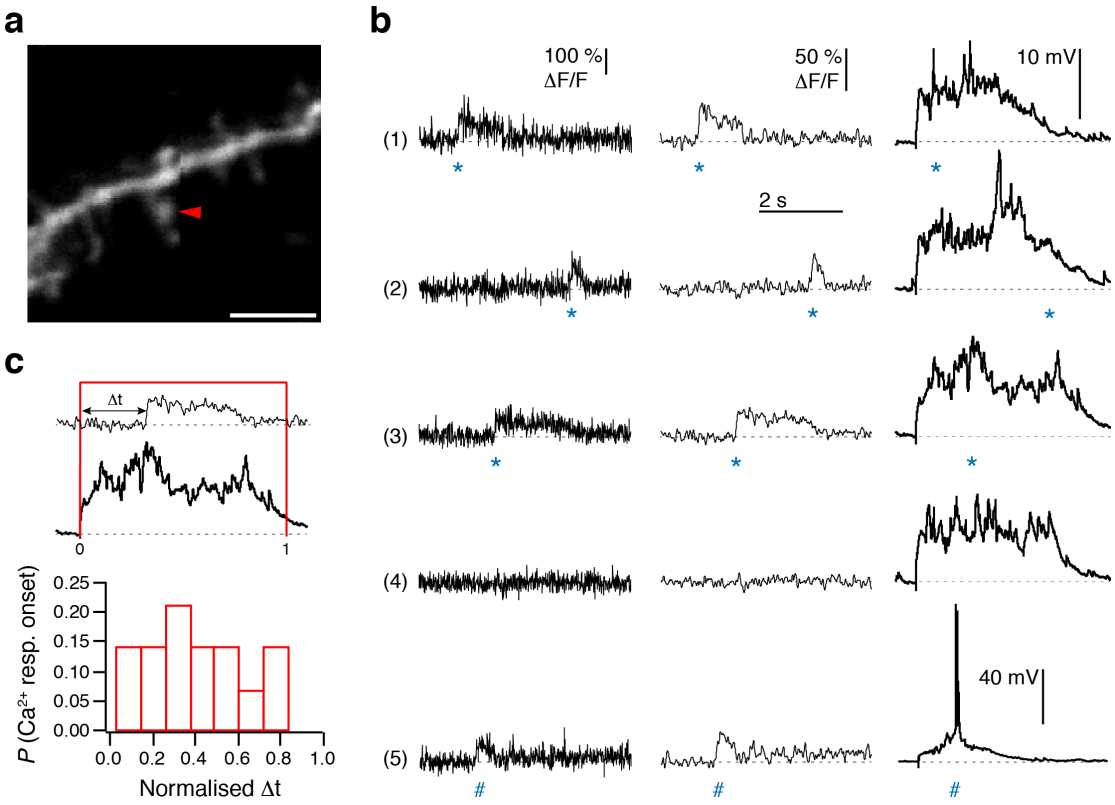

Figure 14 Temporal distribution of spontaneous Ca^{2+} transients during Up states. **(a)** Medial section from a basal dendrite (scale bar: 5 um). The red arrowhead marks the imaged spine. **(b)** Representative spontaneous Ca^{2+} transients: Shown are the raw traces (left), filtered traces (8-point binominal smoothing filter) (middle), and the corresponding evoked Up states (right). Responses 1-4 probably reflect synaptic activations (marked with a blue asterix), while response 5 is due to a back-propagating action potential (blue hashtag). **(c)** Probability histogram of normalised onset latencies of Ca^{2+} transients (based on 14 responses during subthreshold Up states).

5.4 Discussion

In this chapter, I demonstrated that the average spine Ca^{2+} response evoked by synaptic inputs is boosted during Up states relative to Down states. This finding is consistent with the hypothesis that relates the magnitude of the postsynaptic Ca^{2+} response to the sign of changes in synaptic efficacy (Lisman 1989; Artola and Singer 1993), since I earlier showed (*chapter 3*) that subthreshold inputs paired with Down states did not cause a change synaptic weight, while subthreshold Up state pairings resulted in synaptic depression. Moreover, positive single-spike and burst pairings with synaptic inputs during Up states may preserve or potentiate that input, respectively (*chapter 3*). Such action potentials can, also during Up state periods, backpropagate into the dendritic tree and result in associated Ca^{2+} transients in dendritic shafts and spines (*Fig. 13b*). Moreover, backpropagating actions potentials, which are boosted during Up states (Waters and Helmchen 2004), can trigger supralinear increases in spine Ca^{2+} when paired with synaptic input (Yuste and Denk 1995; Schiller, Schiller, and Clapham 1998). Therefore, one may expect that the input-spike pairings during Up states are associated with even larger Ca^{2+} elevations in spines compared to subthreshold Up state pairings. Such a simple relationship between spine Ca^{2+} and the different types of synaptic plasticity that were investigated in this thesis is intriguing. Next, it will

have to be examined if a moderate Ca^{2+} elevation during Up states is necessary for the induction of synaptic weakening. Moreover, even if this turns out to be true for the plasticity protocols used here, more natural scenarios will also need to be considered, in which other converging signals could determine the magnitude and sign of synaptic plasticity (Wang et al. 2005; Nevian and Sakmann 2006). Next-generation SHG voltage imaging of dendritic spines during plasticity induction promises a significant advancement in our understanding of these processes.

In the next part of this chapter, I studied spontaneous spine Ca^{2+} transients during Up states in entorhinal cortex. Only one study I am aware of has previously investigated the spatiotemporal dynamics of spontaneous spine Ca^{2+} transients during Up states (Chen et al. 2013). In this in vivo study, principal cells in auditory cortex were studied under anaesthesia. The authors report a relatively low average number of nonclustered spine activations per Up state. Moreover, *Chen et al.* report the surprising finding that spine activation declines during the Up state period. In contrast, in entorhinal cortex, I found a relatively uniform distribution of onset latencies of spine activations (based on Ca^{2+} measurements; see *Fig. 14*). A possible explanation for this discrepancy is a methodical one: The slow kinetics of the calcium indicator (OGB-1) that was used by *Chen et al.* together with relatively short Up state durations could have made it difficult to resolve multiple activations of the

same spine during individual Up states. This could explain the observed decline of spine activations if only the onset latency of the very first Ca^{2+} transient was quantified. Therefore, the number of spine activations, especially towards the end the Up state, might have been underestimated. In any case, spine Ca^{2+} transients seem to occur throughout the Up state period. It will now need to be investigated whether the boost of the average spine Ca^{2+} transient during Up states that was found here is simply the consequence of a relatively constant Up-state associated depolarisation, or if more localised events of synaptic cooperativity cause distinct spine Ca^{2+} transients during Up states, which could ultimately trigger synaptic weakening. Such a cooperation of inputs could be a stochastic event or it could be the result of a coordinated activation of functional synaptic clusters (Kastellakis et al. 2015). Future experiments involving fast Ca^{2+} imaging of entire dendrites using, for example, the remote-focusing technology will have to reveal if such sophisticated nonlinear dendritic computations exist in this context.

6 General discussion and conclusions

I characterised a form of synaptic depression that is mediated by cortical slow-wave activity. Since plasticity was measured for approximately twenty-minutes after pairing, I here referred to this reduction in synaptic strength as *synaptic weakening*. However, there was no indication synapses would recover towards the end of the recording time. For synaptic weakening to occur, subthreshold synaptic inputs needed to coincide with Up states. I continued to demonstrate that Ca^{2+} transients in dendritic spines are boosted during Up states relative to Down states, and that synaptic weakening depends, at least partially, on NMDARs and GSK3β. Finally, it was found that positively input-correlated postsynaptic spiking during Up states can prevent synaptic weakening, and perhaps even lead to synaptic potentiation.

Up states are generated by local recurrent excitation (Sanchez-Vives and McCormick 2000; Compte et al. 2003; Shu, Hasenstaub, and McCormick 2003). I here also demonstrated, using paired recordings from layer III pyramidal neurons, that synapses that naturally contribute to this excitation, due to spontaneous presynaptic Up state spiking, can undergo synaptic weakening. This could provide a network-centred, homeostatic regulation of synaptic strength. A homeostatic renormalisation of synapses during sleep is

the key proposal of the synaptic homeostasis hypothesis (Tononi and Cirelli 2003; Tononi and Cirelli 2006). Clear evidence-based mechanisms supporting this idea have been missing. Interestingly, the mechanism of synaptic weakening during slow-wave activity characterised in this thesis does not seem to dependent on postsynaptic spiking. This could assure a location-independence within the dendritic tree, as opposed to STDP-based mechanisms, which are naturally constrained by the 'reach' of the back-propagating action potential.

All experiments in this thesis are based on acute-slice preparations from mice that were juvenile or in early adolescence, a time of intense learning that exhibits extensive spine turnover and synaptic pruning (Bhatt, Zhang, and Gan 2009). Such early developmental stages also show high SWA and it is conceivable that a selective elimination of synapses is a consequence of extreme synaptic weakening as described here. Consistent with this idea, GSK3β has been suggested to play a role in synaptic pruning via its involvement in NMDAR-dependent synaptic depression (Bradley et al. 2012).

While a function for GSK3β in synaptic plasticity has been convincingly demonstrated, there are also evidence for an implication in various aspects of learning and memory. Mice with a heterozygous GSK3β knockout or more localised inhibition exhibited impairments in fear (Kimura et al. 2008; Chew et al. 2015), reward (Wu et al. 2011) and long-term spatial memory (Kimura et

al. 2008). Some found negative effects on memory retrieval (Chew et al. 2015), while others observed impaired reconsolidation of memories (Kimura et al. 2008; Wu et al. 2011). Although a clear picture of the role of GSK3β in learning and memory is still emerging, its involvement in sleep-dependent synaptic weakening could be a crucial underlying process. Interestingly, a dysregulation of GSK-3β activity has been linked to the β-amyloid pathology in Alzheimer's Disease (AD). Moreover, a recent study has associated the β-amyloid pathology with impaired hippocampus-dependent memory consolidation via the intermediate factor of impaired cortical slow-wave activity (Mander et al. 2015). Impaired synaptic weakening due to a dysregulation of GSK-3β might contribute to such abnormalities in slow-wave activity and memory consolidation associated with AD.

It will now be paramount to investigate if mechanisms similar to synaptic weakening exist in different brain regions and cell types – preferably, *in vivo*. Moreover, the activity-dependence of synaptic weakening suggests that synapses are not proportionally downscaled during slow-wave activity. The effect of such a non-uniform synaptic depression on the information stored in neural circuits will have to be examined.

7 References

Amzica, F., Steriade, M., 1995. Short- and long-range neuronal synchronization of the slow (< 1 Hz) cortical oscillation. J. Neurophysiol. 73, 20–38.

Artola, A., Singer, W., 1993. Long-term depression of excitatory synaptic transmission and its relationship to long-term potentiation. Trends Neurosci. 16, 480–487.

Bain, J., Plater, L., Elliott, M., Shpiro, N., Hastie, C.J., McLauchlan, H., Klevernic, I., Arthur, J.S.C., Alessi, D.R., Cohen, P., 2007. The selectivity of protein kinase inhibitors: a further update. Biochem. J. 408, 297–315.

Barrionuevo, G., Schottler, F., Lynch, G., 1980. The effects of repetitive low frequency stimulation on control and “potentiated” synaptic responses in the hippocampus. Life Sci. 27, 2385–2391.

Battaglia, F.P., Benchenane, K., Sirota, A., Pennartz, C.M.A., Wiener, S.I., 2011. The hippocampus: hub of brain network communication for memory. Trends Cogn. Sci. 15, 310–318.

Bhatt, D.H., Zhang, S., Gan, W.-B., 2009. Dendritic spine dynamics. Annu. Rev. Physiol. 71, 261–282.

Bi, G.Q., Poo, M.M., 1998. Synaptic modifications in cultured hippocampal neurons: dependence on spike timing, synaptic strength, and postsynaptic cell type. J. Neurosci. Off. J. Soc. Neurosci. 18, 10464–10472.

Birtoli, B., Ulrich, D., 2004. Firing mode-dependent synaptic plasticity in rat neocortical pyramidal neurons. J. Neurosci. Off. J. Soc. Neurosci. 24, 4935–4940.

Bliss, T.V., Gardner-Medwin, A.R., 1973. Long-lasting potentiation of synaptic transmission in the dentate area of the unanaestetized rabbit following stimulation of the perforant path. J. Physiol. 232, 357–374.

Bliss, T.V., Lømo, T., 1973. Long-lasting potentiation of synaptic transmission in the dentate area of the anaesthetized rabbit following stimulation of the perforant path. J. Physiol. 232, 331–356.

Born, J., Rasch, B., Gais, S., 2006. Sleep to remember. Neurosci. Rev. J. Bringing Neurobiol. Neurol. Psychiatry 12, 410–424.

Botcherby, E.J., Juskaitis, R., Booth, M.J., Wilson, T., 2007. Aberration-free optical refocusing in high numerical aperture microscopy. Opt. Lett. 32, 2007–2009.

Botcherby, E.J., Smith, C.W., Kohl, M.M., Débarre, D., Booth, M.J., Juškaitis, R., Paulsen, O., Wilson, T., 2012. Aberration-free three-dimensional multiphoton imaging of neuronal activity at kHz rates. Proc. Natl. Acad. Sci. 109, 2919–2924.

Bradley, C.A., Peineau, S., Taghibiglou, C., Nicolas, C.S., Whitcomb, D.J., Bortolotto, Z.A., Kaang, B.-K., Cho, K., Wang, Y.T., Collingridge, G.L., 2012. A pivotal role of GSK-3 in synaptic plasticity. Front. Mol. Neurosci. 5.

Buhry, L., Azizi, A.H., Cheng, S., 2011. Reactivation, replay, and preplay: how it might all fit together. Neural Plast. 2011, 203462.

Bukalo, O., Campanac, E., Hoffman, D.A., Fields, R.D., 2013. Synaptic plasticity by antidromic firing during hippocampal network oscillations. Proc. Natl. Acad. Sci. U. S. A. 110, 5175–5180.

Buzsáki, G., 1989. Two-stage model of memory trace formation: a role for "noisy" brain states. Neuroscience 31, 551–570.

Buzsáki, G., Horváth, Z., Urioste, R., Hetke, J., Wise, K., 1992. High-frequency network oscillation in the hippocampus. Science 256, 1025–1027.

Campagnola, P.J., Wei, M.D., Lewis, A., Loew, L.M., 1999. High-resolution nonlinear optical imaging of live cells by second harmonic generation. Biophys. J. 77, 3341–3349.

Canto, C.B., Wouterlood, F.G., Witter, M.P., 2008. What does the anatomical organization of the entorhinal cortex tell us? Neural Plast. 2008, 381243.

Chen, X., Rochefort, N.L., Sakmann, B., Konnerth, A., 2013. Reactivation of the Same Synapses during Spontaneous Up States and Sensory Stimuli. Cell Rep. 4, 31–39.

Cheong, M.Y., Yun, S.H., Mook-Jung, I., Kang, Y., Jung, M.W., 2002. Induction of homosynaptic long-term depression in entorhinal cortex. Brain Res. 954, 308–310.

Chew, B., Ryu, J.R., Ng, T., Ma, D., Dasgupta, A., Neo, S.H., Zhao, J., Zhong, Z., Bichler, Z., Sajikumar, S., Goh, E.L.K., 2015. Lentiviral silencing of GSK-3β in adult dentate gyrus impairs contextual fear memory and synaptic plasticity. Front. Behav. Neurosci. 9.

Cho, K., Kemp, N., Noel, J., Aggleton, J.P., Brown, M.W., Bashir, Z.I., 2000. A new form of long-term depression in the perirhinal cortex. Nat. Neurosci. 3, 150–156.

Chrobak, J.J., Buzsáki, G., 1996. High-frequency oscillations in the output networks of the hippocampal-entorhinal axis of the freely behaving rat. J. Neurosci. Off. J. Soc. Neurosci. 16, 3056–3066.

Cirelli, C., 2005. A molecular window on sleep: changes in gene expression between sleep and wakefulness. Neurosci. Rev. J. Bringing Neurobiol. Neurol. Psychiatry 11, 63–74.

Cissé, Y., Crochet, S., Timofeev, I., Steriade, M., 2004. Synaptic enhancement induced through callosal pathways in cat association cortex. J. Neurophysiol. 92, 3221–3232.

Clopath, C., Gerstner, W., 2010. Voltage and Spike Timing Interact in STDP - A Unified Model. Front. Synaptic Neurosci. 2, 25.

Collingridge, G.L., Peineau, S., Howland, J.G., Wang, Y.T., 2010. Long-term depression in the CNS. Nat. Rev. Neurosci. 11, 459–473.

Compte, A., Sanchez-Vives, M.V., McCormick, D.A., Wang, X.-J., 2003. Cellular and network mechanisms of slow oscillatory activity (<1 Hz) and wave propagations in a cortical network model. J. Neurophysiol. 89, 2707–2725.

Crochet, S., Fuentealba, P., Cissé, Y., Timofeev, I., Steriade, M., 2006. Synaptic Plasticity in Local Cortical Network In Vivo and Its Modulation by the Level of Neuronal Activity. Cereb. Cortex 16, 618–631.

Cunningham, M.O., Pervouchine, D.D., Racca, C., Kopell, N.J., Davies, C.H., Jones, R.S.G., Traub, R.D., Whittington, M.A., 2006. Neuronal metabolism governs cortical network response state. Proc. Natl. Acad. Sci. 103, 5597–5601.

Czarnecki, A., Birtoli, B., Ulrich, D., 2007. Cellular mechanisms of burst firing-mediated long-term depression in rat neocortical pyramidal cells. J. Physiol. 578, 471–479.

de Vivo, L., Faraguna, U., Nelson, A.B., Pfister-Genskow, M., Klapperich, M.E., Tononi, G., Cirelli, C., 2014. Developmental Patterns of Sleep Slow Wave Activity and Synaptic Density in Adolescent Mice. Sleep 37, 689–700.

Dewachter, I., Ris, L., Jaworski, T., Seymour, C.M., Kremer, A., Borghgraef, P., De Vijver, H., Godaux, E., Van Leuven, F., 2009. GSK3ß, a centre-staged kinase in neuropsychiatric disorders, modulates long term memory by inhibitory phosphorylation at Serine-9. Neurobiol. Dis., Biomarkers of Neuropsychiatric Disease 35, 193–200.

Dhillon, A., Jones, R.S., 2000. Laminar differences in recurrent excitatory transmission in the rat entorhinal cortex in vitro. Neuroscience 99, 413–422.

Diekelmann, S., Born, J., 2010. The memory function of sleep. Nat. Rev. Neurosci. 11, 114–126.

Dombeck, D.A., Sacconi, L., Blanchard-Desce, M., Webb, W.W., 2005. Optical recording of fast neuronal membrane potential transients in

acute mammalian brain slices by second-harmonic generation microscopy. J. Neurophysiol. 94, 3628–3636.

Dudek, S.M., Bear, M.F., 1992. Homosynaptic long-term depression in area CA1 of hippocampus and effects of N-methyl-D-aspartate receptor blockade. Proc. Natl. Acad. Sci. U. S. A. 89, 4363–4367.

Dupret, D., Csicsvari, J., 2012. The medial entorhinal cortex keeps Up. Nat. Neurosci. 15, 1471–1472.

Ellenbogen, J.M., Hu, P.T., Payne, J.D., Titone, D., Walker, M.P., 2007. Human relational memory requires time and sleep. Proc. Natl. Acad. Sci. 104, 7723–7728.

Faber, D.S., Korn, H., 1991. Applicability of the coefficient of variation method for analyzing synaptic plasticity. Biophys. J. 60, 1288–1294.

Feldman, D.E., 2000. Timing-Based LTP and LTD at Vertical Inputs to Layer II/III Pyramidal Cells in Rat Barrel Cortex. Neuron 27, 45–56.

Fischer, S., Hallschmid, M., Elsner, A.L., Born, J., 2002. Sleep forms memory for finger skills. Proc. Natl. Acad. Sci. U. S. A. 99, 11987–11991.

Frank, M.G., 2013. Why I am not shy: a reply to Tononi and Cirelli. Neural Plast. 2013, 394946.

Gloveli, T., Schmitz, D., Empson, R.M., Dugladze, T., Heinemann, U., 1997. Morphological and electrophysiological characterization of layer III cells of the medial entorhinal cortex of the rat. Neuroscience 77, 629–648.

Grienberger, C., Konnerth, A., 2012. Imaging calcium in neurons. Neuron 73, 862–885.

Gustafsson, B., Wigström, H., Abraham, W.C., Huang, Y.Y., 1987. Long-term potentiation in the hippocampus using depolarizing current pulses as the conditioning stimulus to single volley synaptic potentials. J. Neurosci. Off. J. Soc. Neurosci. 7, 774–780.

Hahn, T.T.G., McFarland, J.M., Berberich, S., Sakmann, B., Mehta, M.R., 2012. Spontaneous persistent activity in entorhinal cortex modulates cortico-hippocampal interaction in vivo. Nat. Neurosci. 15, 1531–1538.

Hanlon, E.C., Faraguna, U., Vyazovskiy, V.V., Tononi, G., Cirelli, C., 2009. Effects of skilled training on sleep slow wave activity and cortical gene expression in the rat. Sleep 32, 719–729.

Hao, J., Oertner, T.G., 2012. Depolarization gates spine calcium transients and spike-timing-dependent potentiation. Curr. Opin. Neurobiol. 22, 509–515.

Harnett, M.T., Makara, J.K., Spruston, N., Kath, W.L., Magee, J.C., 2012. Synaptic amplification by dendritic spines enhances input cooperativity. Nature 491, 599–602.

Hayama, T., Noguchi, J., Watanabe, S., Takahashi, N., Hayashi-Takagi, A., Ellis-Davies, G.C.R., Matsuzaki, M., Kasai, H., 2013. GABA promotes

the competitive selection of dendritic spines by controlling local Ca2+ signaling. Nat. Neurosci. 16, 1409–1416.
Hebb, D.O., 1949. Organization of Behavior: a Neuropsychological Theory. John Wiley, New York.
Higley, M.J., 2014. Localized GABAergic inhibition of dendritic Ca2+ signalling. Nat. Rev. Neurosci. 15, 567–572.
Higley, M.J., Sabatini, B.L., 2012. Calcium signaling in dendritic spines. Cold Spring Harb. Perspect. Biol. 4, a005686.
Hinard, V., Mikhail, C., Pradervand, S., Curie, T., Houtkooper, R.H., Auwerx, J., Franken, P., Tafti, M., 2012. Key electrophysiological, molecular, and metabolic signatures of sleep and wakefulness revealed in primary cortical cultures. J. Neurosci. Off. J. Soc. Neurosci. 32, 12506–12517.
Holmgren, C., Harkany, T., Svennenfors, B., Zilberter, Y., 2003. Pyramidal cell communication within local networks in layer 2/3 of rat neocortex. J. Physiol. 551, 139–153.
Kastellakis, G., Cai, D.J., Mednick, S.C., Silva, A.J., Poirazi, P., 2015. Synaptic clustering within dendrites: An emerging theory of memory formation. Prog. Neurobiol. 126, 19–35.
Kelso, S.R., Ganong, A.H., Brown, T.H., 1986. Hebbian synapses in hippocampus. Proc. Natl. Acad. Sci. U. S. A. 83, 5326–5330.
Kemp, N., Bashir, Z.I., 2001. Long-term depression: a cascade of induction and expression mechanisms. Prog. Neurobiol. 65, 339–365.
Kimura, T., Yamashita, S., Nakao, S., Park, J.-M., Murayama, M., Mizoroki, T., Yoshiike, Y., Sahara, N., Takashima, A., 2008. GSK-3beta is required for memory reconsolidation in adult brain. PloS One 3, e3540.
Kirkwood, A., Bear, M.F., 1994. Homosynaptic long-term depression in the visual cortex. J. Neurosci. Off. J. Soc. Neurosci. 14, 3404–3412.
Kleindienst, T., Winnubst, J., Roth-Alpermann, C., Bonhoeffer, T., Lohmann, C., 2011. Activity-Dependent Clustering of Functional Synaptic Inputs on Developing Hippocampal Dendrites. Neuron 72, 1012–1024.
Kruskal, P.B., Li, L., MacLean, J.N., 2013. Circuit reactivation dynamically regulates synaptic plasticity in neocortex. Nat. Commun. 4, 2574.
Kudrimoti, H.S., Barnes, C.A., McNaughton, B.L., 1999. Reactivation of hippocampal cell assemblies: effects of behavioral state, experience, and EEG dynamics. J. Neurosci. Off. J. Soc. Neurosci. 19, 4090–4101.
Lanté, F., Toledo-Salas, J.-C., Ondrejcak, T., Rowan, M.J., Ulrich, D., 2011. Removal of synaptic Ca^2+-permeable AMPA receptors during sleep. J. Neurosci. Off. J. Soc. Neurosci. 31, 3953–3961.
Larkman, A., Hannay, T., Stratford, K., Jack, J., 1992. Presynaptic release probability influences the locus of long-term potentiation. Nature 360, 70–73.

Lau, K.F., Miller, C.C., Anderton, B.H., Shaw, P.C., 1999. Expression analysis of glycogen synthase kinase-3 in human tissues. J. Pept. Res. Off. J. Am. Pept. Soc. 54, 85–91.

Levy, R.B., Reyes, A.D., 2012. Spatial profile of excitatory and inhibitory synaptic connectivity in mouse primary auditory cortex. J. Neurosci. 32, 5609–5619.

Levy, W.B., Steward, O., 1979. Synapses as associative memory elements in the hippocampal formation. Brain Res. 175, 233–245.

Lewis, P.A., Durrant, S.J., 2011. Overlapping memory replay during sleep builds cognitive schemata. Trends Cogn. Sci. 15, 343–351.

Lisman, J., 1989. A mechanism for the Hebb and the anti-Hebb processes underlying learning and memory. Proc. Natl. Acad. Sci. U. S. A. 86, 9574–9578.

Liu, Z.-W., Faraguna, U., Cirelli, C., Tononi, G., Gao, X.-B., 2010. Direct Evidence for Wake-Related Increases and Sleep-Related Decreases in Synaptic Strength in Rodent Cortex. J. Neurosci. 30, 8671–8675.

Lynch, G.S., Dunwiddie, T., Gribkoff, V., 1977. Heterosynaptic depression: a postsynaptic correlate of long-term potentiation. Nature 266, 737–739.

Mander, B.A., Marks, S.M., Vogel, J.W., Rao, V., Lu, B., Saletin, J.M., Ancoli-Israel, S., Jagust, W.J., Walker, M.P., 2015. β-amyloid disrupts human NREM slow waves and related hippocampus-dependent memory consolidation. Nat. Neurosci. 18, 1051–1057.

Mann, E.O., Kohl, M.M., Paulsen, O., 2009. Distinct roles of GABA(A) and GABA(B) receptors in balancing and terminating persistent cortical activity. J. Neurosci. Off. J. Soc. Neurosci. 29, 7513–7518.

Maret, S., Faraguna, U., Nelson, A.B., Cirelli, C., Tononi, G., 2011. Sleep and waking modulate spine turnover in the adolescent mouse cortex. Nat. Neurosci. 14, 1418–1420.

Markram, H., Lübke, J., Frotscher, M., Sakmann, B., 1997. Regulation of synaptic efficacy by coincidence of postsynaptic APs and EPSPs. Science 275, 213–215.

Marshall, L., Helgadóttir, H., Mölle, M., Born, J., 2006. Boosting slow oscillations during sleep potentiates memory. Nature 444, 610–613.

Massey, P.V., Bashir, Z.I., 2007. Long-term depression: multiple forms and implications for brain function. Trends Neurosci. 30, 176–184.

Massimini, M., Huber, R., Ferrarelli, F., Hill, S., Tononi, G., 2004. The Sleep Slow Oscillation as a Traveling Wave. J. Neurosci. 24, 6862–6870.

McBride, T.J., Rodriguez-Contreras, A., Trinh, A., Bailey, R., Debello, W.M., 2008. Learning drives differential clustering of axodendritic contacts in the barn owl auditory system. J. Neurosci. Off. J. Soc. Neurosci. 28, 6960–6973.

McClelland, J.L., McNaughton, B.L., O'Reilly, R.C., 1995. Why there are complementary learning systems in the hippocampus and neocortex: insights from the successes and failures of connectionist models of learning and memory. Psychol. Rev. 102, 419–457.

Mulkey, R.M., Malenka, R.C., 1992. Mechanisms underlying induction of homosynaptic long-term depression in area CA1 of the hippocampus. Neuron 9, 967–975.

Nelson, A.B., Faraguna, U., Zoltan, J.T., Tononi, G., Cirelli, C., 2013. Sleep Patterns and Homeostatic Mechanisms in Adolescent Mice. Brain Sci. 3, 318–343.

Neske, G.T., Patrick, S.L., Connors, B.W., 2015. Contributions of diverse excitatory and inhibitory neurons to recurrent network activity in cerebral cortex. J. Neurosci. Off. J. Soc. Neurosci. 35, 1089–1105.

Nevian, T., Sakmann, B., 2006. Spine Ca2+ signaling in spike-timing-dependent plasticity. J. Neurosci. Off. J. Soc. Neurosci. 26, 11001–11013.

Olcese, U., Esser, S.K., Tononi, G., 2010. Sleep and synaptic renormalization: a computational study. J. Neurophysiol. 104, 3476–3493.

Papatheodoropoulos, C., 2008. A possible role of ectopic action potentials in the in vitro hippocampal sharp wave-ripple complexes. Neuroscience 157, 495–501.

Peineau, S., Taghibiglou, C., Bradley, C., Wong, T.P., Liu, L., Lu, J., Lo, E., Wu, D., Saule, E., Bouschet, T., Matthews, P., Isaac, J.T.R., Bortolotto, Z.A., Wang, Y.T., Collingridge, G.L., 2007. LTP Inhibits LTD in the Hippocampus via Regulation of GSK3β. Neuron 53, 703–717.

Peterka, D.S., Takahashi, H., Yuste, R., 2011. Imaging voltage in neurons. Neuron 69, 9–21.

Plihal, W., Born, J., 1999. Effects of early and late nocturnal sleep on priming and spatial memory. Psychophysiology 36, 571–582.

Plihal, W., Born, J., 1997. Effects of early and late nocturnal sleep on declarative and procedural memory. J. Cogn. Neurosci. 9, 534–547.

Rama, S., Vetrivel, L., Semyanov, A., 2010. Second-harmonic generation voltage imaging at subcellular resolution in rat hippocampal slices. J. Biophotonics 3, 784–790.

Rasch, B., Born, J., 2013. About sleep's role in memory. Physiol. Rev. 93, 681–766.

Reig, R., Zerlaut, Y., Vergara, R., Destexhe, A., Sanchez-Vives, M.V., 2015. Gain Modulation of Synaptic Inputs by Network State in Auditory Cortex In Vivo. J. Neurosci. 35, 2689–2702.

Sabatini, B.L., Maravall, M., Svoboda, K., 2001. Ca(2+) signaling in dendritic spines. Curr. Opin. Neurobiol. 11, 349–356.

Sacconi, L., Dombeck, D.A., Webb, W.W., 2006. Overcoming photodamage in second-harmonic generation microscopy: real-time optical recording of neuronal action potentials. Proc. Natl. Acad. Sci. U. S. A. 103, 3124–3129.

Sanchez-Vives, M.V., McCormick, D.A., 2000. Cellular and network mechanisms of rhythmic recurrent activity in neocortex. Nat. Neurosci. 3, 1027–1034.

Sastry, B.R., Goh, J.W., Auyeung, A., 1986. Associative induction of posttetanic and long-term potentiation in CA1 neurons of rat hippocampus. Science 232, 988–990.

Schiller, J., Schiller, Y., Clapham, D.E., 1998. NMDA receptors amplify calcium influx into dendritic spines during associative pre- and postsynaptic activation. Nat. Neurosci. 1, 114–118.

Seong, H.J., Behnia, R., Carter, A.G., 2014. Impact of subthreshold membrane potential on synaptic responses at dendritic spines of layer 5 pyramidal neurons in the prefrontal cortex. J. Neurophysiol. 111, 1960–1972.

Shahab, L., Plattner, F., Irvine, E.E., Cummings, D.M., Edwards, F.A., 2014. Dynamic range of GSK3α not GSK3β is essential for bidirectional synaptic plasticity at hippocampal CA3-CA1 synapses. Hippocampus 1413-1416.

Sheroziya, M.G., Halbach, O. von B. und, Unsicker, K., Egorov, A.V., 2009. Spontaneous Bursting Activity in the Developing Entorhinal Cortex. J. Neurosci. 29, 12131–12144.

Shu, Y., Hasenstaub, A., Duque, A., Yu, Y., McCormick, D.A., 2006. Modulation of intracortical synaptic potentials by presynaptic somatic membrane potential. Nature 441, 761–765.

Shu, Y., Hasenstaub, A., McCormick, D.A., 2003. Turning on and off recurrent balanced cortical activity. Nature 423, 288–293.

Siapas, A.G., Wilson, M.A., 1998. Coordinated interactions between hippocampal ripples and cortical spindles during slow-wave sleep. Neuron 21, 1123–1128.

Siegel, J.M., 2001. The REM sleep-memory consolidation hypothesis. Science 294, 1058–1063.

Sirota, A., Csicsvari, J., Buhl, D., Buzsáki, G., 2003. Communication between neocortex and hippocampus during sleep in rodents. Proc. Natl. Acad. Sci. U. S. A. 100, 2065–2069.

Sjöström, P.J., Turrigiano, G.G., Nelson, S.B., 2004. Endocannabinoid-dependent neocortical layer-5 LTD in the absence of postsynaptic spiking. J. Neurophysiol. 92, 3338–3343.

Sjöström, P.J., Turrigiano, G.G., Nelson, S.B., 2003. Neocortical LTD via coincident activation of presynaptic NMDA and cannabinoid receptors. Neuron 39, 641–654.

Staresina, B.P., Bergmann, T.O., Bonnefond, M., van der Meij, R., Jensen, O., Deuker, L., Elger, C.E., Axmacher, N., Fell, J., 2015. Hierarchical nesting of slow oscillations, spindles and ripples in the human hippocampus during sleep. Nat. Neurosci. advance online publication.

Steriade, M., Nunez, A., Amzica, F., 1993. A novel slow (< 1 Hz) oscillation of neocortical neurons in vivo: depolarizing and hyperpolarizing components. J. Neurosci. 13, 3252–3265.

Steriade, M., Timofeev, I., 2003. Neuronal plasticity in thalamocortical networks during sleep and waking oscillations. Neuron 37, 563–576.

Steriade, M., Timofeev, I., Grenier, F., 2001. Natural waking and sleep states: a view from inside neocortical neurons. J. Neurophysiol. 85, 1969–1985.

Stickgold, R., James, L., Hobson, J.A., 2000. Visual discrimination learning requires sleep after training. Nat. Neurosci. 3, 1237–1238.

Stickgold, R., Walker, M.P., 2013. Sleep-dependent memory triage: evolving generalization through selective processing. Nat. Neurosci. 16, 139–145.

Takahashi, N., Kitamura, K., Matsuo, N., Mayford, M., Kano, M., Matsuki, N., Ikegaya, Y., 2012. Locally synchronized synaptic inputs. Science 335, 353–356.

Thomas, M.J., Malenka, R.C., Bonci, A., 2000. Modulation of long-term depression by dopamine in the mesolimbic system. J. Neurosci. Off. J. Soc. Neurosci. 20, 5581–5586.

Timofeev, I., 2011. Neuronal plasticity and thalamocortical sleep and waking oscillations. Prog. Brain Res. 193, 121–144.

Tononi, G., Cirelli, C., 2014. Sleep and the price of plasticity: from synaptic and cellular homeostasis to memory consolidation and integration. Neuron 81, 12–34.

Tononi, G., Cirelli, C., 2006. Sleep function and synaptic homeostasis. Sleep Med. Rev. 10, 49–62.

Tononi, G., Cirelli, C., 2003. Sleep and synaptic homeostasis: a hypothesis. Brain Res. Bull. 62, 143–150.

van der Linden, S., Lopes da Silva, F.H., 1998. Comparison of the electrophysiology and morphology of layers III and II neurons of the rat medial entorhinal cortex in vitro. Eur. J. Neurosci. 10, 1479–1489.

van Haeften, T., Baks-te-Bulte, L., Goede, P.H., Wouterlood, F.G., Witter, M.P., 2003. Morphological and numerical analysis of synaptic interactions between neurons in deep and superficial layers of the entorhinal cortex of the rat. Hippocampus 13, 943–952.

Vyazovskiy, V.V., Cirelli, C., Pfister-Genskow, M., Faraguna, U., Tononi, G., 2008. Molecular and electrophysiological evidence for net synaptic potentiation in wake and depression in sleep. Nat. Neurosci. 11, 200–208.

Vyazovskiy, V.V., Delogu, A., 2014. NREM and REM Sleep: Complementary Roles in Recovery after Wakefulness. Neurosci. Rev. J. Bringing Neurobiol. Neurol. Psychiatry 20, 203–219.

Wagner, U., Gais, S., Born, J., 2001. Emotional memory formation is enhanced across sleep intervals with high amounts of rapid eye movement sleep. Learn. Mem. Cold Spring Harb. N 8, 112–119.

Walker, M.P., Brakefield, T., Morgan, A., Hobson, J.A., Stickgold, R., 2002. Practice with sleep makes perfect: sleep-dependent motor skill learning. Neuron 35, 205–211.

Wang, H.-X., Gerkin, R.C., Nauen, D.W., Bi, G.-Q., 2005. Coactivation and timing-dependent integration of synaptic potentiation and depression. Nat. Neurosci. 8, 187–193.

Waters, J., Helmchen, F., 2004. Boosting of action potential backpropagation by neocortical network activity in vivo. J. Neurosci. Off. J. Soc. Neurosci. 24, 11127–11136.

Wilson, M.A., McNaughton, B.L., 1994. Reactivation of hippocampal ensemble memories during sleep. Science 265, 676–679.

Woodgett, J.R., 1990. Molecular cloning and expression of glycogen synthase kinase-3/factor A. EMBO J. 9, 2431–2438.

Wu, P., Xue, Y.-X., Ding, Z.-B., Xue, L.-F., Xu, C.-M., Lu, L., 2011. Glycogen synthase kinase 3β in the basolateral amygdala is critical for the reconsolidation of cocaine reward memory. J. Neurochem. 118, 113–125.

Yang, G., Gan, W.-B., 2012. Sleep contributes to dendritic spine formation and elimination in the developing mouse somatosensory cortex. Dev. Neurobiol. 72, 1391–1398.

Yang, G., Lai, C.S.W., Cichon, J., Ma, L., Li, W., Gan, W.-B., 2014. Sleep promotes branch-specific formation of dendritic spines after learning. Science 344, 1173–1178.

Yang, S.N., Tang, Y.G., Zucker, R.S., 1999. Selective induction of LTP and LTD by postsynaptic [Ca2+]i elevation. J. Neurophysiol. 81, 781–787.

Yao, H.-B., Shaw, P.-C., Wong, C.-C., Wan, D.C.-C., 2002. Expression of glycogen synthase kinase-3 isoforms in mouse tissues and their transcription in the brain. J. Chem. Neuroanat. 23, 291–297.

Yasuda, R., Nimchinsky, E.A., Scheuss, V., Pologruto, T.A., Oertner, T.G., Sabatini, B.L., Svoboda, K., 2004. Imaging calcium concentration dynamics in small neuronal compartments. Sci. STKE Signal Transduct. Knowl. Environ. 2004, pl5.

Yuste, R., Denk, W., 1995. Dendritic spines as basic functional units of neuronal integration. Nature 375, 682–684.

Zhang, L.I., Tao, H.W., Holt, C.E., Harris, W.A., Poo, M., 1998. A critical window for cooperation and competition among developing retinotectal synapses. Nature 395, 37–44.

8 Appendix

8.1 Morphology and location of representative MEC layer III principal cells

8.1.1 Single-cell plasticity experiment

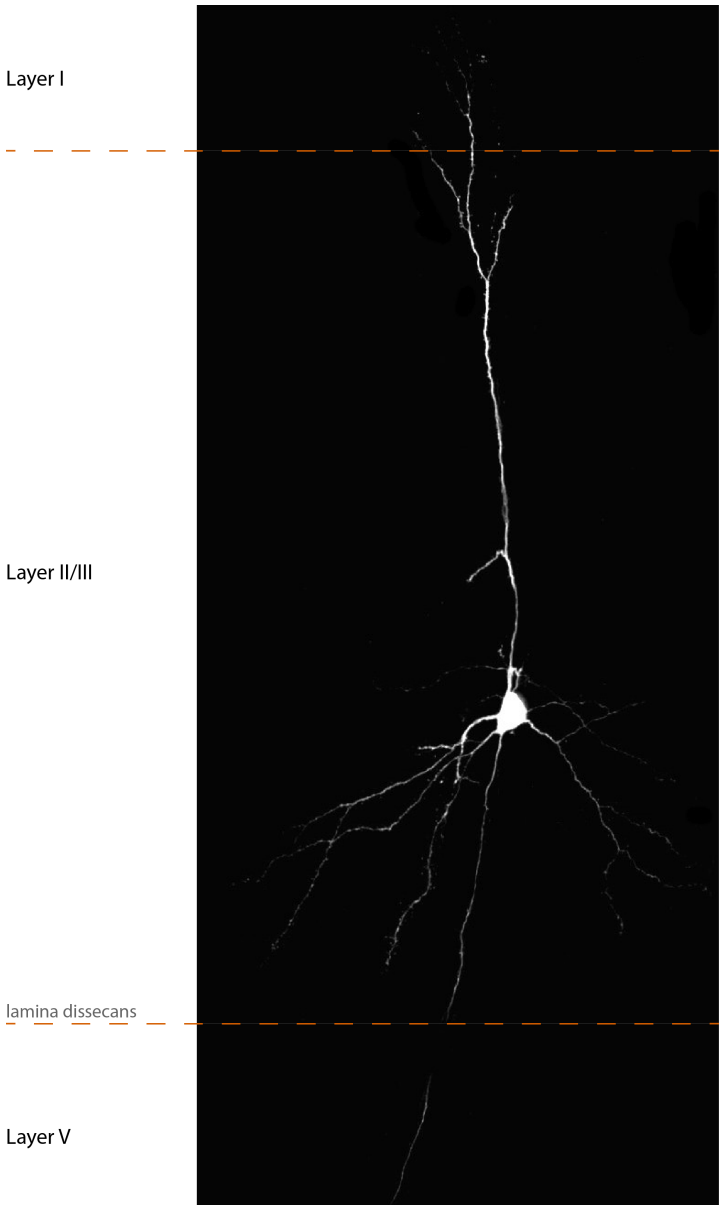

8.1.2 Dual-cell plasticity experiment

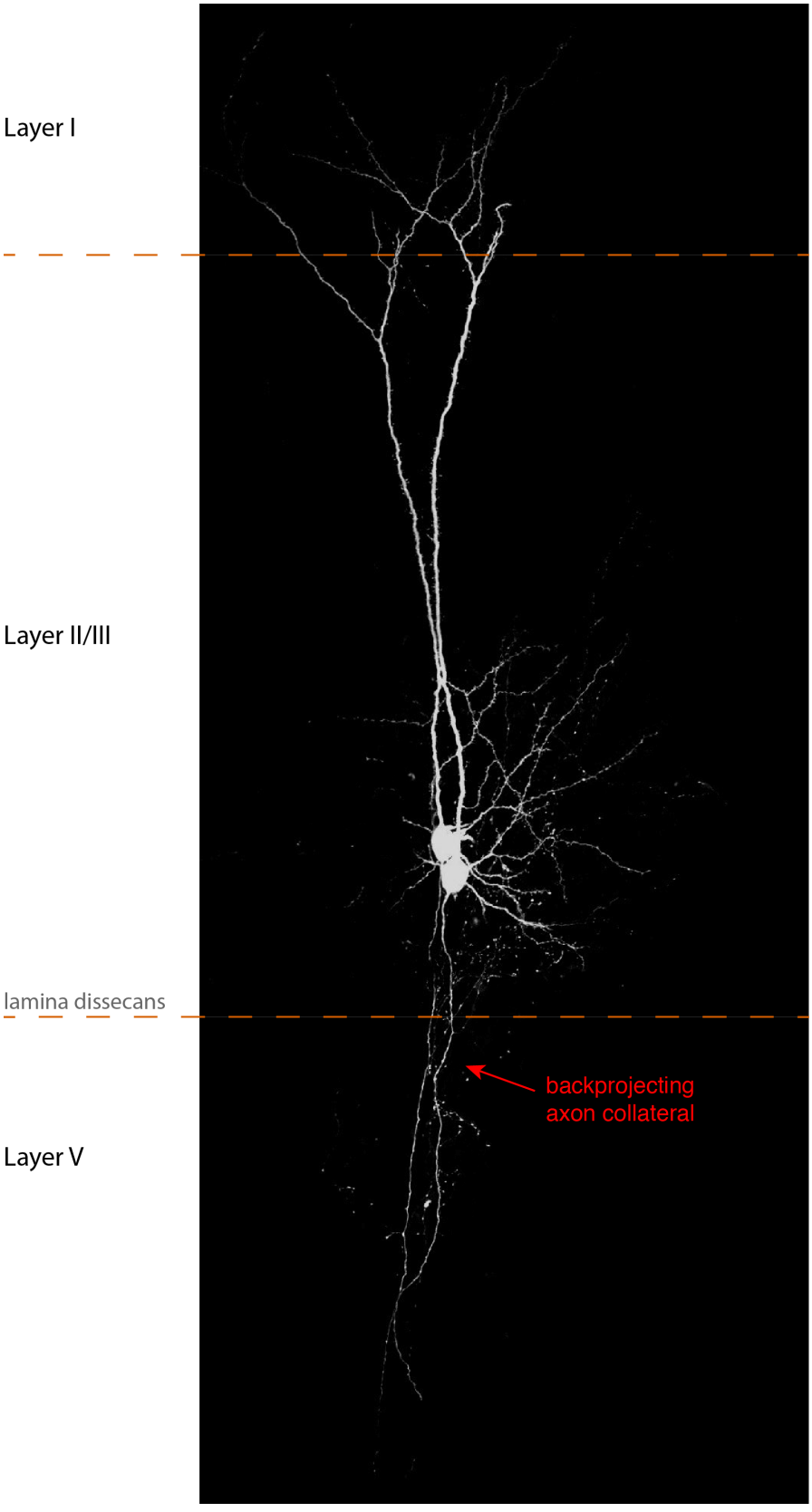

8.1.3 Spine Ca^{2+} imaging experiment